Confidential

Accuracy of Liquid Level Sensors

Report

MMS Contract No.: 1435-01-05-CT-39120

FOR
UNITED STATES DEPARTMENT OF THE INTERIOR
MINERALS MANAGEMENT SERVICE

This report has been reviewed by the Minerals Management Service and approved for publication. Approval does not signify that the contents necessarily reflect the views and policies of the Service, nor does mention of trade names or commercial products constitute endorsement or recommendation for use.

JANUARY 25 2007

California Office:
2240 Vineyard Avenue
Escondido, CA 92029
Phone: (760) 737-3505
Fax: (760) 737-0232

Texas Office:
9835B Whithorn Drive
Houston, TX 77095
Phone: (281) 858-8090
Fax: (281) 858-8898

Rev. No.	Rev. Date	Rev. Description	Issued By	Checked By	Engineer Approval	BMT-SMS Approval
01	7/25/06	Draft	CC/AL	IP	SA	
02	12/15/06	Released to client for comments	IP			IP
03	1/25/07	Final	IP			IP

PROPRIETARY NOTICE

This publication contains information that has been derived in part from proprietary data from **BMT Scientific Marine Services, Inc**. This information is provided to assist in evaluating the numerical simulation results as a part of this study for Mineral Management Service. Publication of this information does not convey any rights to reproduce it or to use it for any purpose other than in connection with the evaluation of the scope of the work defined for this study.

Table of Contents

Table of Figures

Table of Tables

1. Introduction

The United States Department of the Interior – Minerals Management Service, hereafter referred to as **MMS** has indicated that the common MMS practice of sampling the liquid levels in the tanks on some Spars and TLPs using 20-second intervals might not be correct and this sample rate needs to be reevaluated. BMT Scientific Marine Services Inc and BMT Fluid Mechanic Ltd, hereafter referred to as **BMT** conducted such an evaluation based on real measurements of the fluid level in the ballast tanks (full-scale data from two Spars and a TLP) and the conclusions are generalized based on Computational Fluid Dynamics (CFD) analyses.

The MMS primary interest is in evaluating the liquid motions in the tanks based on the 6 degrees of freedom motions of the platform.

2. Background

Any motion of the free surface inside a partially confine volume (container) is called *sloshing.* The cause of sloshing can be <u>any</u> disturbance. It can be induced by motions of the container or by pressure disturbance above the free surface or inside the body of liquid. In ship and oil production industry, the global motions of the vessels and thus the containers, as well as the pressure burst due to discharge of oil in an oil-gas-water separator are typical examples that can cause liquid sloshing. Depending on the container shape (see Figure 1) and the type of liquid commotion (see Figure 2 and Figure 3), the free liquid surface can experience a variety of motions including simple and complex, planar and non-planar, symmetric and asymmetric, as well as periodic or chaotic motions.

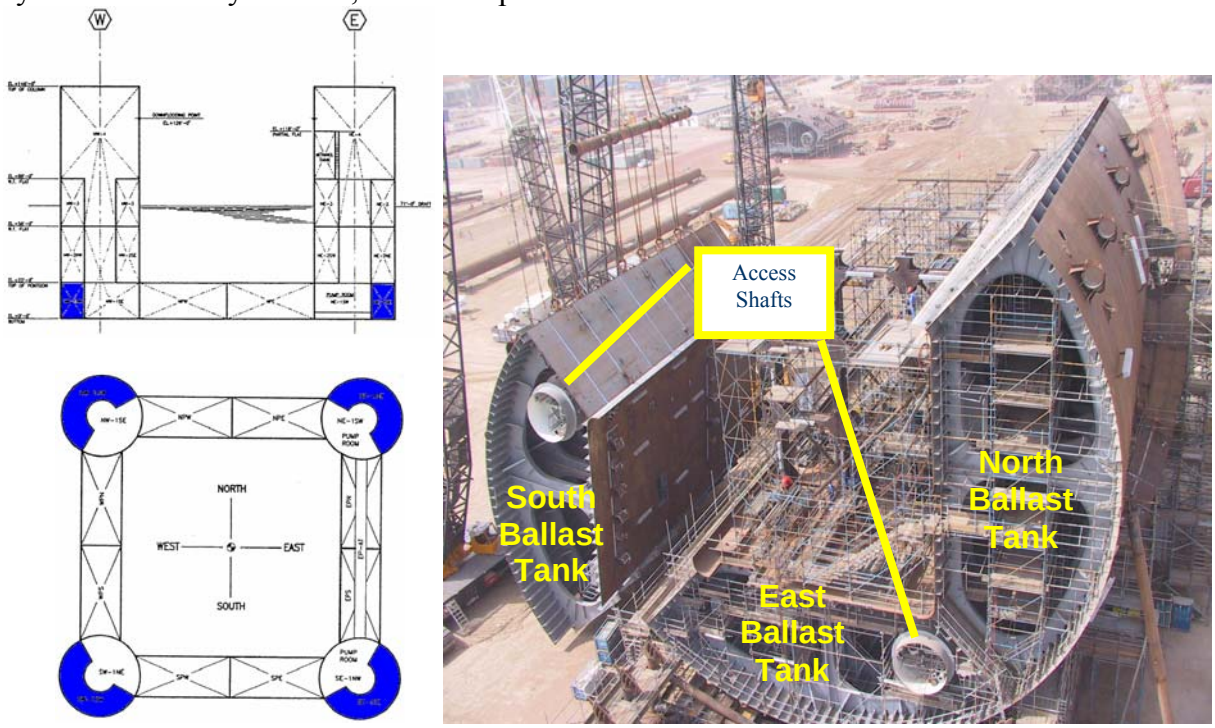

Figure 1: Typical cross-sections of the tanks on TPL (left) and SPAR (right) platforms

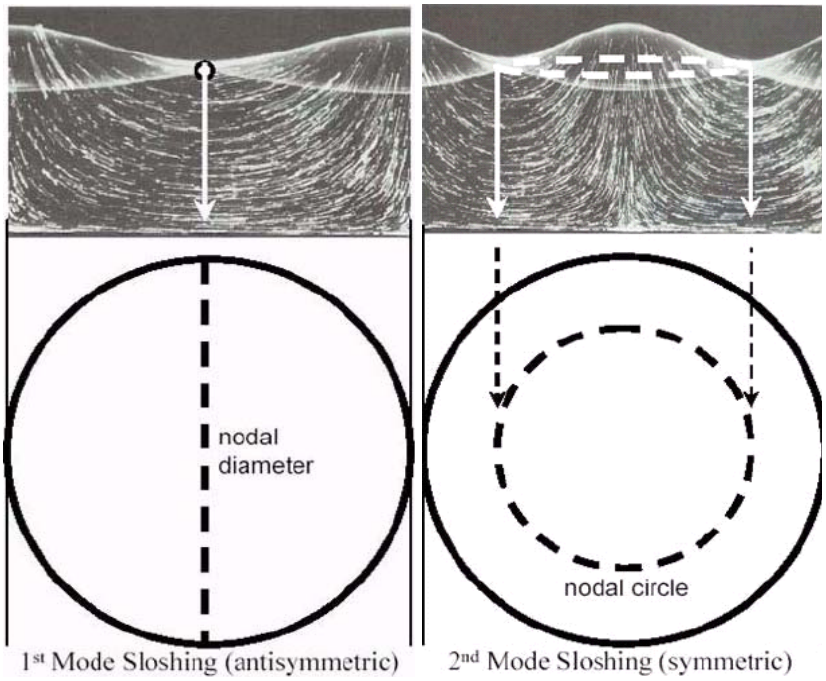

Figure 2: (a)1st and (b) 2nd sloshing modes in a cylindrical vertical container (Van Dyke, 1982)

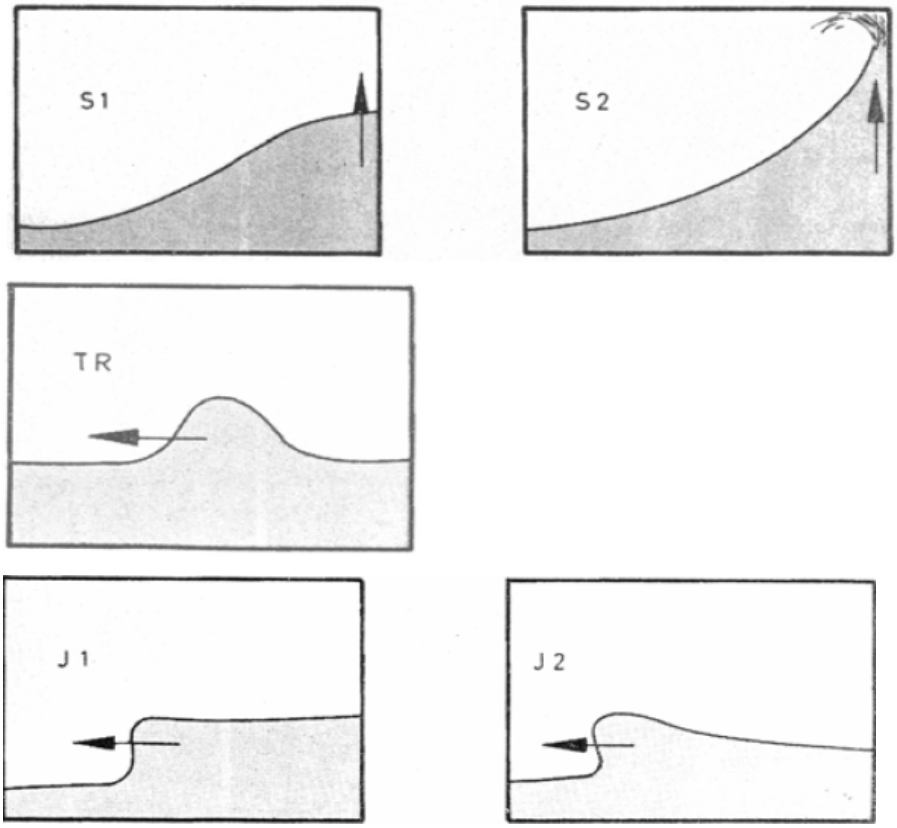

Figure 3: Variety of sloshing: (S1&S2) standing wave; (TR) progresive wave; (J1&J2) hydraulic jump

The crux of the liquid sloshing problem is the evaluation of the natural frequencies of the free liquid surface and loads (localized pressure and global forces) on the liquid holding container and on the whole vessel. The liquid sloshing may negatively affect dynamic stability of a vessel if resonant coupling occurs, or sloshing can be the main cause of annoying false alarms.

Sloshing flows in engineering applications are complex in types and also strongly nonlinear in most cases, thus they are difficult to solve analytically (Ibrahim, 2005; Faltinsen *et al.*, 2003) Analytical solutions are limited to regular shapes of the containers, such as rectangular, cylindrical, and spherical. Interestingly, the nature of sloshing flows is better understood for cylindrical than rectangular tanks. In practice, the tank geometry can be of any shape that can be far from either rectangular or cylindrical tanks (see Figure 1).

Motion of a liquid in a tank has two most important components: (a) one component is proportional with the tank motion, thus it is caused by forced oscillations of the tank boundaries; (b) another component represents the free-surface liquid motions, which occurs spontaneously when the liquid is left alone and goes through the process of finding its equilibrium condition.

Although sloshing has an infinite number of natural frequencies, it is most likely that only the lowest modes will be excited by the tank motions. As a result, usually only these frequencies are investigated. That is, only possible oscillations near the lowest natural frequencies that can be predicted by linear equations for fluid motion are investigated (Lamb, 1997). The equation for the first mode natural frequency in a rectangular tank of length "a" and depth of liquid "h" is provided below and visualized in Figure 4:

$$T = 2\pi\sqrt{\frac{a}{g\pi}}\sqrt{\coth(\frac{h\pi}{a})}$$

Assuming that the length of a tank is 60 ft and the liquid depth is 16 ft,

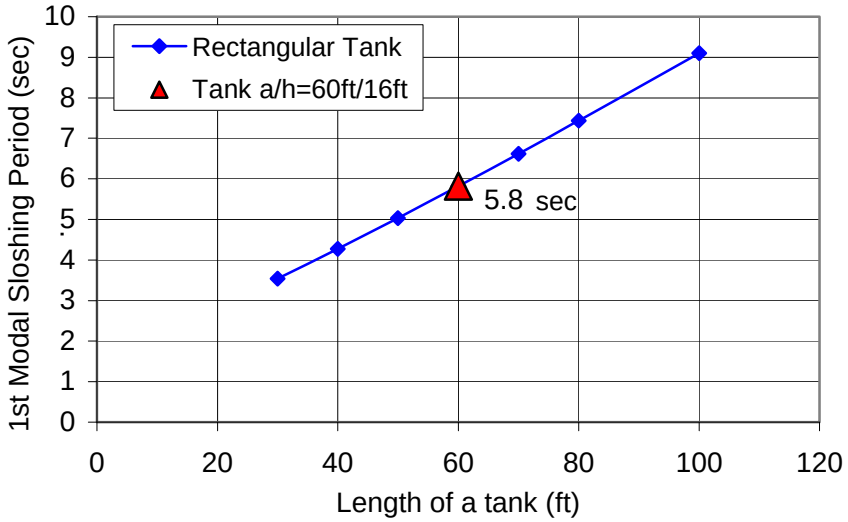

Figure 4: 1st Modal Sloshing Period for Rectangular Tanks

On the other hand, in reality, nonlinear effects play significant role as evident in amplitude jump, parametric resonance, and chaotic motion.

Analytical solutions for sloshing are not only limited by the tank geometry, but also by the type of fluid (viscous and multiphase flows), the amount of liquid in a tank, and the tank compartmentalization, to mention just a few.

Significant progress in numerical modeling of sloshing has been made during the last decade by using computer codes to solve complex problems that are difficult to solve analytically (Ibrahim, 2005).

3. Objectives

It is known that partially filled tanks experience liquid movement that can be observed as motions of the free surface in the form of standing waves or sloshing. In both cases, the liquid motions strongly correlate with the linear and angular motions of the platform, such as surge/sway and roll/pitch if the liquid motion resonant periods are close to the platform motion periods. An example of the correlation between the ballast level and the pitch motion of a Spar platform is shown in Figure 5. High correlation between the Spar pitch and the ballast level is found at 10 seconds (the wave period) and at 40 seconds (the Spar pitch natural period). The ballast level spectrum confirms these findings (see Figure 6). In addition, Figure 6 reveals some small liquid motions in the ballast tank at around 25 and 103 seconds at which the pitch spectral values are insignificant. These liquid motions can be attributed to motions of the Spar other than pitch (most likely due to heave and surge, respectively) and this can be further analyzed using CFD modeling.

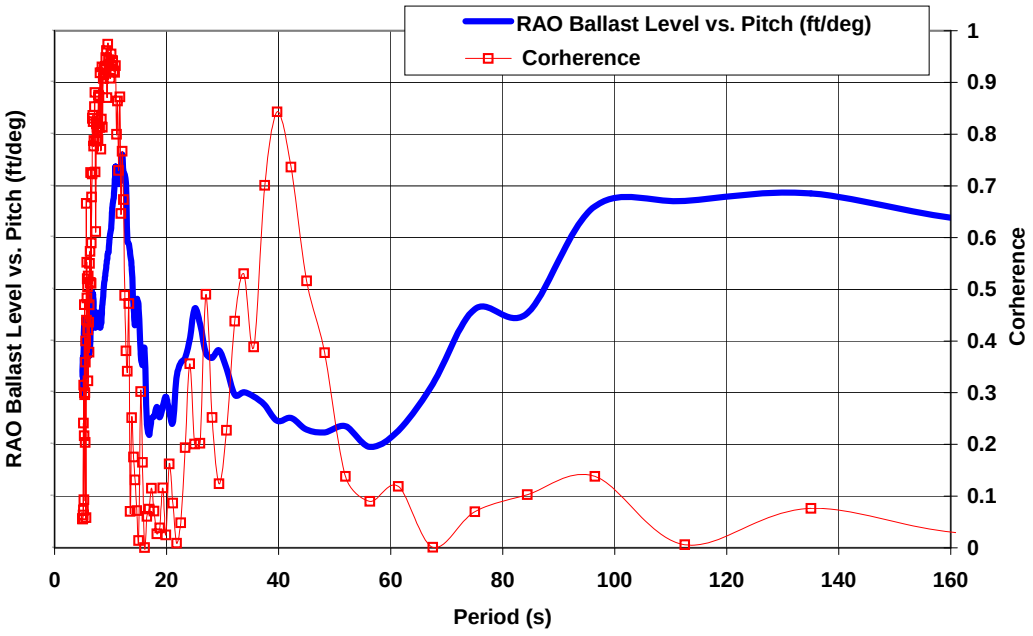

Figure 5: RAO and Coherence between Pitch and Ballast Level (from an existing Spar Platform)

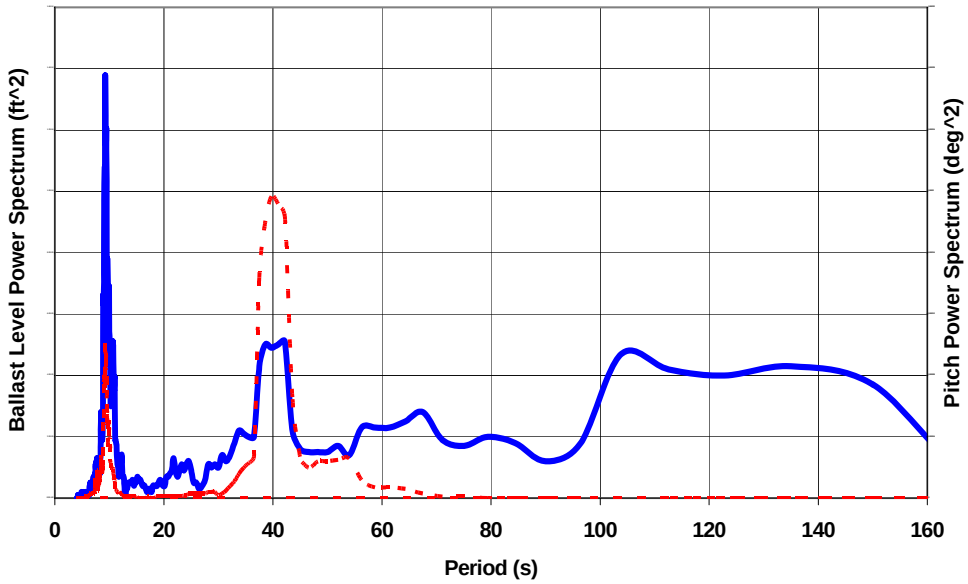

Figure 6: Power Spectra for Ballast Level and Pitch (from an existing Spar Platform)

Similarly to a Spar offshore platform, a TLP motion data are used to the feed the CFD model. The TLP pitch and roll periods are relatively short (3 to 4 seconds) and usually lower than the wave periods (6 to 15 seconds). Thus, the time step for CFD modeling of a TPL tank needs to be much smaller than the time step for a Spar tank.

The sampling rate for full-scale motion and liquid level data varies from platform to platform. The full-scale data we are proposing to use are sampled with the following frequencies, as shown in Table 1

Table 1: Full-Scale Sampling Frequencies For Motions And Liquid Levels

Platform	Liquid Levels	Motions
	sampling frequency (Hz)	
Spar 1	0.5	10
Spar 2	0.5	2
TLP	0.1	1

As it can be seen from Table 1, the sampling frequencies for motions for all three platforms seem to be appropriate for generating inputs for the CFD modeling. The sampling rate of 10 Hz for Spar No. 1 is obviously much higher than needed for this study. The sampling rate of 1 Hz for the TLP could be higher, but we believe that there will not be an aliasing problem for the motion data. Unfortunately, the sampling rates are already implemented in the data acquisition systems and we cannot change them for this study. We will validate the CFD model using the full-scale motion data from one of the spars with better signal to noise ratio.
The sampling rates for the liquid level measurements are much lower (longer sampling time intervals) than the sampling rates for the motion data. However, these relatively low sampling rates for liquid level

measurements in the tanks are at least two to ten times higher than the target sampling rate of 0.05 Hz (20 seconds) that MMS wants to be investigated. Thus, the numerical, CFD model can be validated for the sampling frequencies as high as the sampling rate for the input motion data. The comparisons with the measured liquid level data to evaluate the accuracy of the liquid level sensors are possible only for up to 0.5 Hz. The procedures that will be used in this study are discussed in Section 7.

Using the Spar and TLP full-scale motions, extracted from real measurements, the liquid motion in ballast tanks will be simulated using CFD methods and the liquid level will be predicted at the location where the real liquid level measurement were taken.

Finite volume formulations of the governing Reynolds Averaged Navier Stokes (**RANS**) equations will be solved for six degrees-of-freedom motions. The free surface will be modeled using the volume of fluids (VOF) method. The measured and simulated results will be compared in both the time and frequency domains. This comparison makes it possible to identify the periods where the real measurements might lack accuracy due to inadequate sampling time.

4. Implementation

BMT understands that the accurate measurements of the liquid level in a partially filled tank are crucial for detecting the leakage, overfilling, and the dynamic loading, particularly due to sloshing. These important issues are characterized by completely different time scales (periods). We believe that only careful CFD modeling of this phenomenon, based on accurate real measurements, can lead to the solutions appropriate for defining the liquid level sampling intervals.
Having in mind that CFD modeling is very time demanding, we will provide CFD simulations anticipating a limited number of cases for long runs and all of the cases for short runs. Long and short runs will be in duration of around 1,000 and 200 seconds real, full-scale time, respectively.

5. Scope of Work

5.1. Summary of the Scope of Work

The scope of work is divided into four major tasks as follows:

- Full-scale measurement data acquisition and designation
- System identification and data preparation for numerical modeling
- Numerical, CFD modeling and simulations
- Data reduction and reporting

5.2. Detailed scope of work

Each of the identified tasks covers the following steps in achieving the final goal:

Task A

- Identify full-scale global motions of oil platforms at the location of a liquid tank.

Task B

- Identify characteristic parameters of liquid motion in tanks, such as elevation and global dominant frequency.
- Identify occurrences of sloshing in a tank by watching for transients in full-scale liquid level data using time-frequency detection methods.

Task C

- Build up the CFD model to match the geometry of the tanks,
- Validate the CFD model, using the best full-scale measurements,
- Compare the CFD results with the full-scale measurements,
- Perform CFD calculations for multi-point sensor system arrangement at locations around the circumference of the tank for the best matching case.
-

- Perform sensitivity test using the CFD model for different levels of tank filling for a pre-selected tank.

Task D

- Compare full-scale and simulated data and identify degree of confidence for the numerical modeling
- Compare simulated data for different liquid levels in a tank and identify trend in the results.

6. Methodology

6.1. Full Scale Data

The BMT Scientific Marine Services Inc pioneering Integrated Marine Monitoring Systems (IMMS) have been provided to over 30 deepwater platforms across the Gulf of Mexico, West Africa, Newfoundland, and Brazil. Some of the deepwater Offshore Platforms in the Gulf of Mexico equipped with the permanent IMMSs are shown in Figure 7. These systems employ field proven technology that integrates all elements of platform monitoring—often operated independently—into a single system, thus ensuring that all operating performance variables can be analyzed together. These systems have been discussed by Edwards *et al.* (2005).
The principal objectives of an IMMS are to provide operational decision support data in real time to platform operators and to produce archived data on a common time base to aid in Forensic Engineering and Integrity management.
The primary function of an IMMS is to provide real-time information in an easy to understand format to the platform operators. The system provides "feedback" in a form and in a time frame that permits the operators to evaluate the impact of their actions on important platform responses. Over a 7 year period, BMT has worked closely with platform operators to develop practical, user friendly screens with functionality that suits their real world requirements.

Some of the Measurement Subsystems that are typically included in a BMT IMMS are:

- *Platform kinematics: accelerations and angular Rates*
- Platform position
- Trim, heel, draft
- *Ballast tank level and volume monitoring and recording*
- Void leak detection
- Wind velocity and direction
- Air gap (wave profile estimation)
- Full depth current profile
- Mooring line tension and payout
- Buoyancy chamber pressure (leak detection)
- Production riser top tension and bending moments
- Production riser stroke
- Steel catenary riser flex joint statics and kinematics

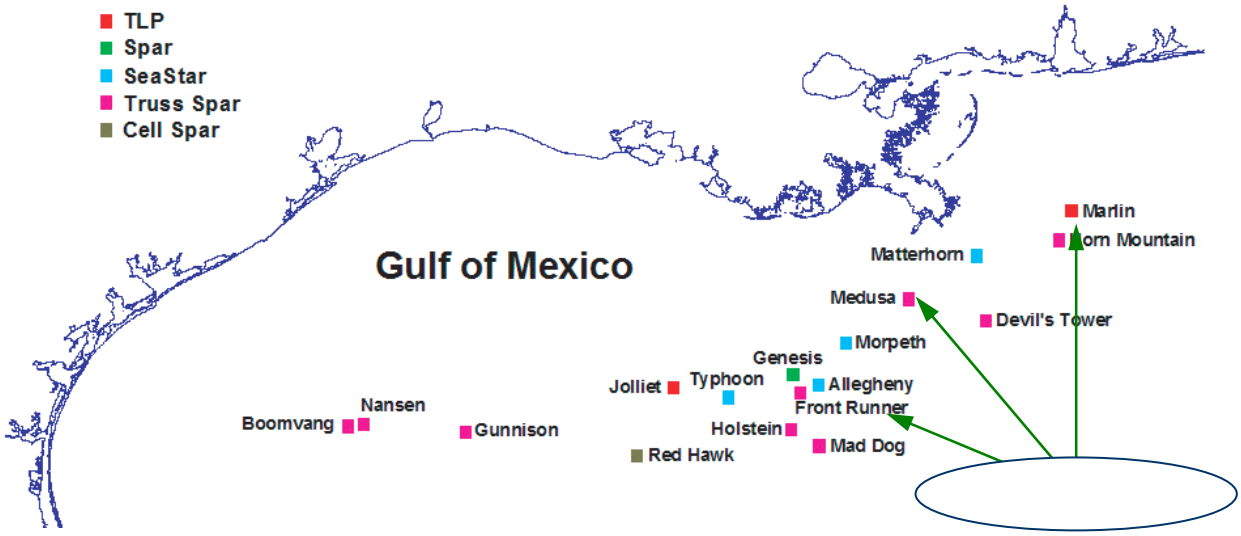

Figure 7: Map Showing some deep-water offshore platforms in the Gulf of Mexico instrumented by BMT (platforms selected for this study are indicated)

For the purpose of the study "*Accuracy of Liquid Level Sensors*", the only available real-time measurements that have been archived on the offshore platforms are the ballast tank levels. Some other tank level data, such as the levels in oil-water-gas separators and fuel tanks either are not permanently recorded or they are not available. Thus, for this study we use measurements of the water level in the ballast tanks to calibrate the effectiveness of the CFD code. After the validation for accuracy, the CFD simulations are further used to address some relevant behaviors of the fluid in the tanks affected by the real, six-degrees of platform motions.

Two types of platforms are selected for liquid level evaluation: spar and TLP. These types of platforms are not only the most typical deepwater platforms but also their principles of operation and effectiveness to sustain in a harsh environment are quite different: Natural responses of a spar are at relatively low frequencies whereas responses of a TLP are at relatively high frequencies; both frequencies are beyond the normal wave frequency range, thus the effects of the platform motion excitation frequencies are minimized.

However, the fluid excitation in the tanks can still be present due to such reasons as shape, orientation, depth, and compartmentalization of a tank. Thus, the geometry of a tank can result in different sloshing natural frequencies. Therefore, by selecting the type of the platform and its six-degrees of motions, it is possible to investigate the behavior of the liquid in the tanks (sloshing) as a function of the tank excitation due to the platform motions.

BP America and Murphy Oil kindly allowed us to use the IMMS archived real-time data for the BP Marlin TLP and the Murphy Medusa and Front Runner spars (see Figure 7).

6.2. Sloshing Event Selection

To our knowledge, there is no a specific record about a significant sloshing in the ballast tanks on any of three selected platforms. The only information that operators care about ballast tanks is the amount of water that is relevant to ballast the platform. Thus, we looked at the two-year historical records for the measured amount of water in the ballast tanks. To validate the CFD code, we decided to focus on the data from the Medusa spar. We followed the following steps to identify a relevant sloshing event:

- Post-process two years of available data based on 1-hour records (around 17,000 records),
- Compare the standard deviations for pitch motion and amount of water and select a few events when both values are above the averages (see Figure 8.
- Narrow down the event when the mean tank level does not change over a noticeable period (see Figure 9); this step is important because the operator might be filling/emptying the tanks, in which case a large standard deviation could be misinterpreted as an indication of significant sloshing.

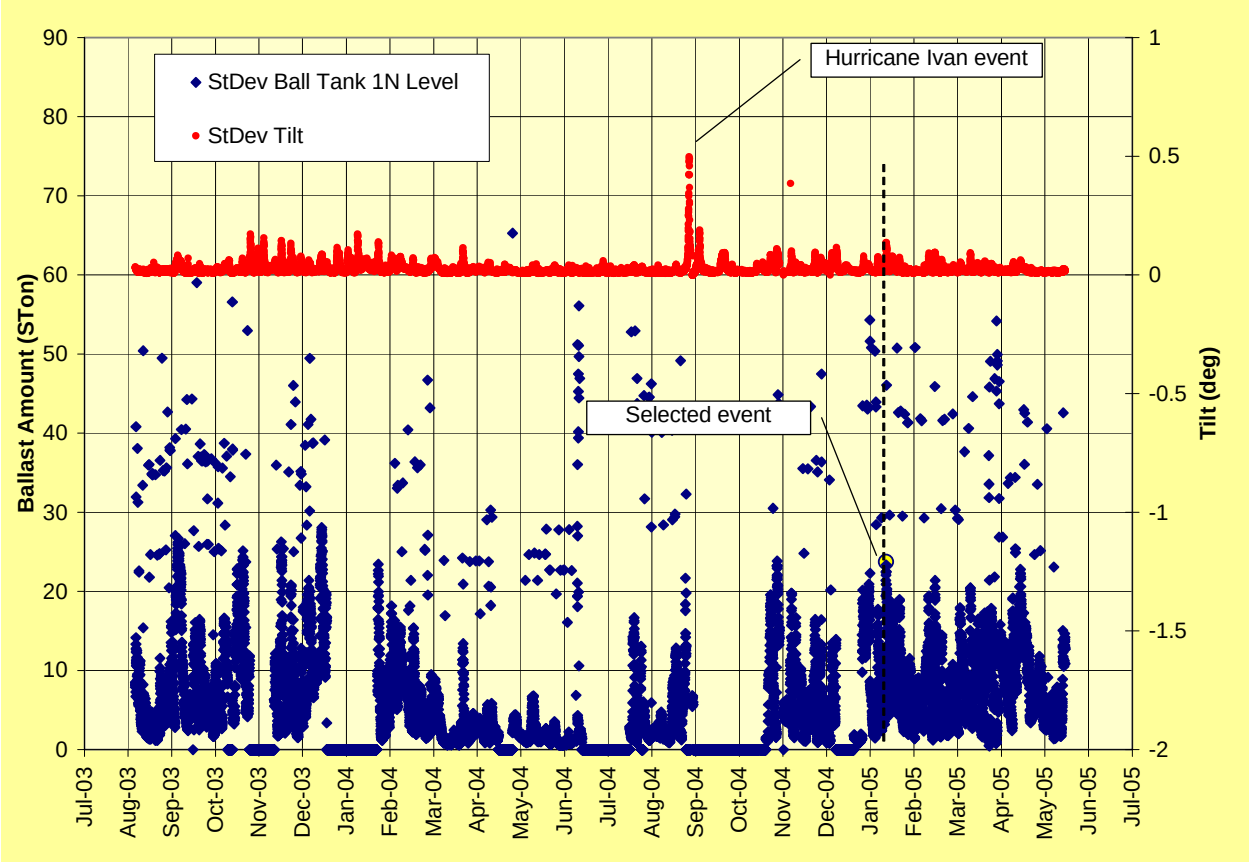

Figure 8: Probable sloshing events in the North Ballast tank on Medusa spar during 2-year period

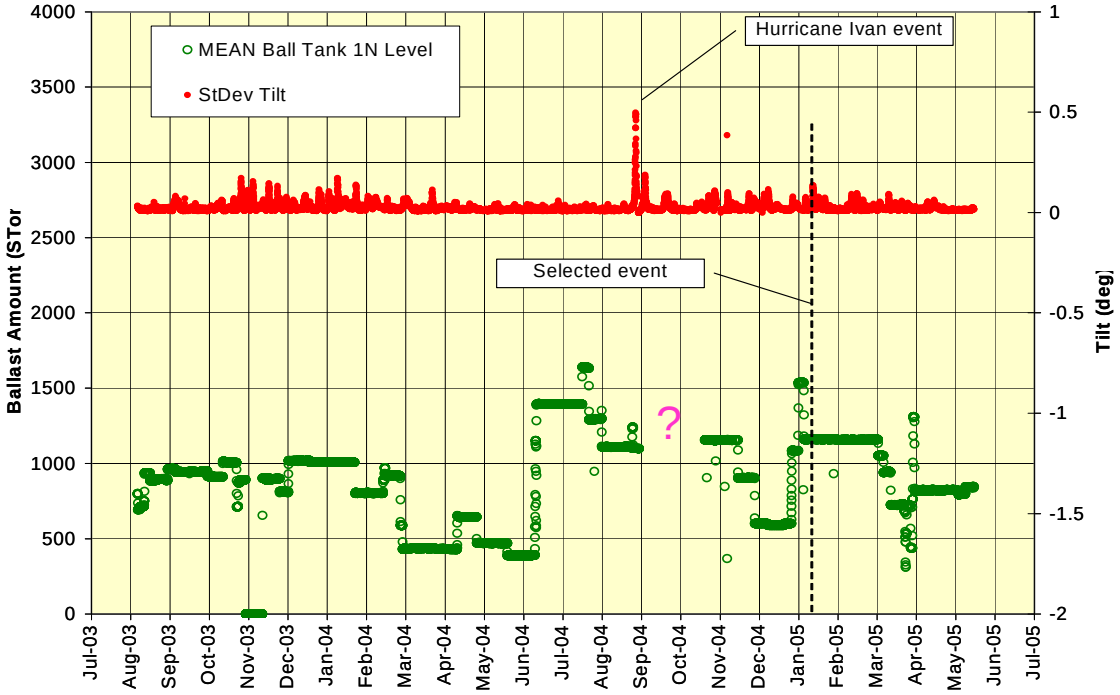

Figure 9:Amount of water in the North ballast tank for the selected sloshing event

Find a case from all available measured data that shows:

- the largest **dynamic** free-surface motions
- the **mean water level** does not change (no ballasting)

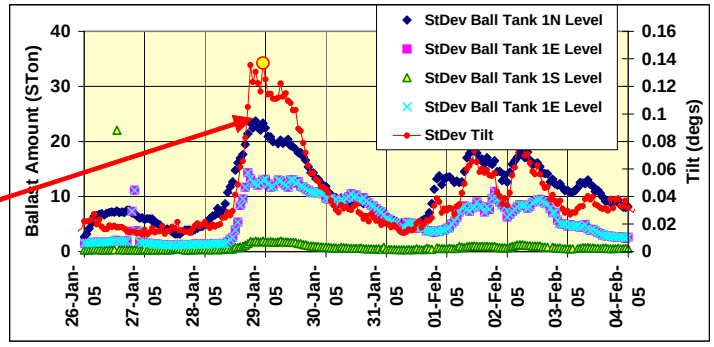

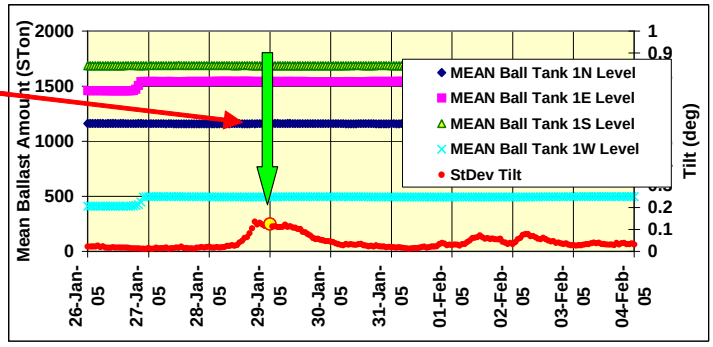

Figure 10: Final confirmation and selection of the sloshing event

Close inspection of Figure 9 reveals that Medusa spar experienced a distant hurricane event in September 2004. During this event, the spar dynamic angular motion (tilt) was noticeably higher than during any other event. This would be a perfect event to study sloshing in tanks, but unfortunately, the ballast control system was disconnected from the IMMS and no fluid level data were recorded during this event. However, another, though much more benign winter storm event on January 29, 2005 was identified (see Figure 10) that could potentially induced sloshing in one of the ballast tanks (see Figure 11). A detailed inspection of the platform motions, particularly the tilt, and the dynamics of the liquid levels in the ballast tanks reveals that sloshing was present as shown in Figure 10 and Figure 12).

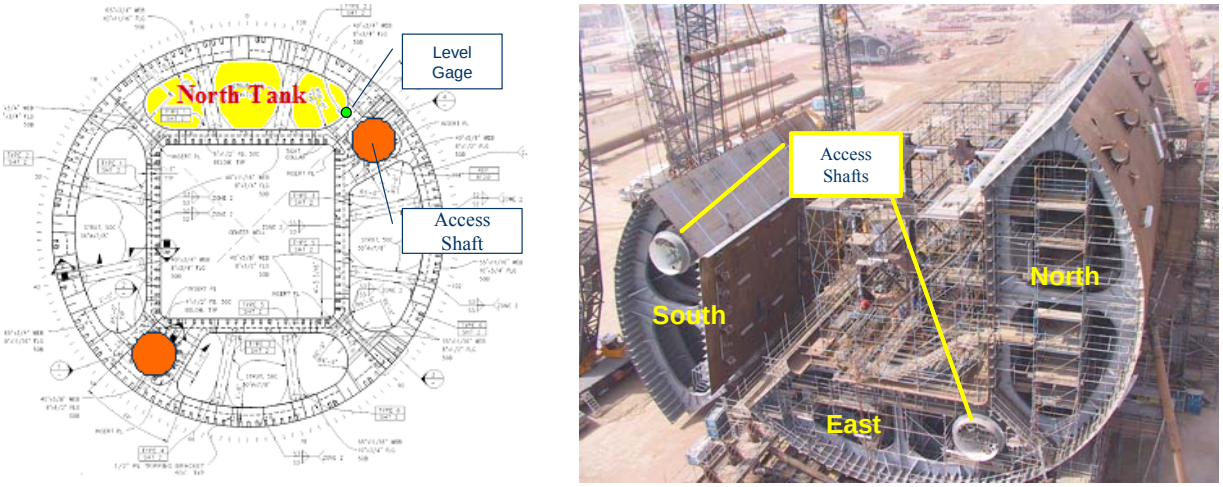

Figure 11: Hard Tank Cross-section on Medusa Spar (left) and the Front Runner Spar Hard Tank Assembly (similar to Medusa Spar)

It is obvious from Figure 12 that platform rolling (rotation around x-axis) is more pronounced than pitching (rotation around y-axis) and it is expected that the liquid motions in either the north or the south ballast tanks would be detectable. Indeed, the largest liquid motions are detected in the north ballast tank (see Figure 10 and Figure 12).

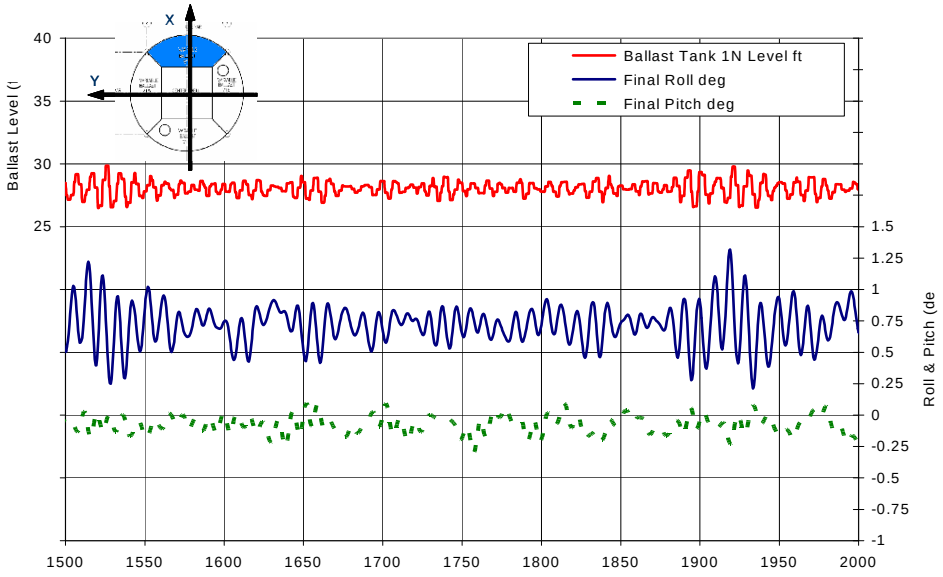

Figure 12: Platform roll and pitch motions and the fluid level fluctuation in the North Ballast Tank

Similarly, the platform swaying (oscillation along the y-axis) is also contributing to liquid excitations in the north ballast tank, but at much lower frequency than the rolling frequency (see Figure 13).

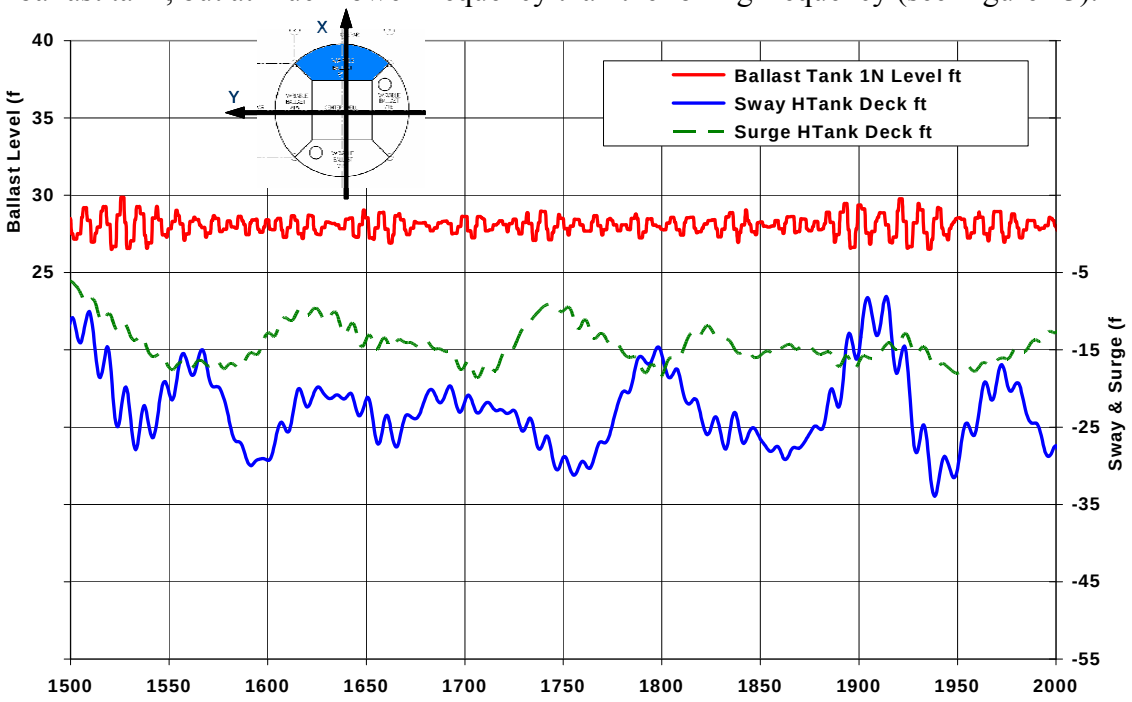

Figure 13: Platform surge and sway motions and the fluid level fluctuation in the North Ballast Tank

It should be noted that the liquid level in the north ballast tank was measured near the vertical bulkhead, on the other side of the NE access shaft (see Figure 11). The measuring probe[1] measures the pressure head at the end of the sense line and the pressure is long time averaged and converted into amount of water in the tank. However, when the measurements are used at higher sampling intervals, dynamics of the water level above the probe can be analyzed.

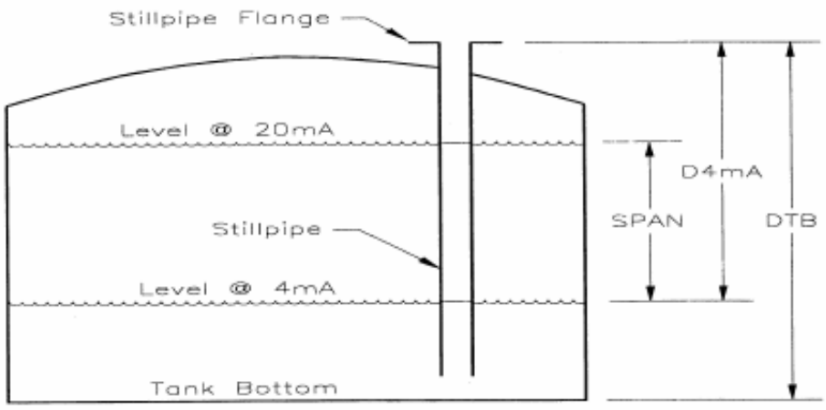

Figure 14: Liquid level measurmen system in ballast tanks

[1] Level Com 100(1) by Technical Marine Service, Inc.

To double check which platform motions are primarily responsible for the liquid sloshing, spectral coherence analyses were also performed, as shown in Figure 15 to Figure 18. Results show that only platform motions roll and sway which are aligned with the direction of waves are responsible for the sloshing in the north ballast tank during this event.

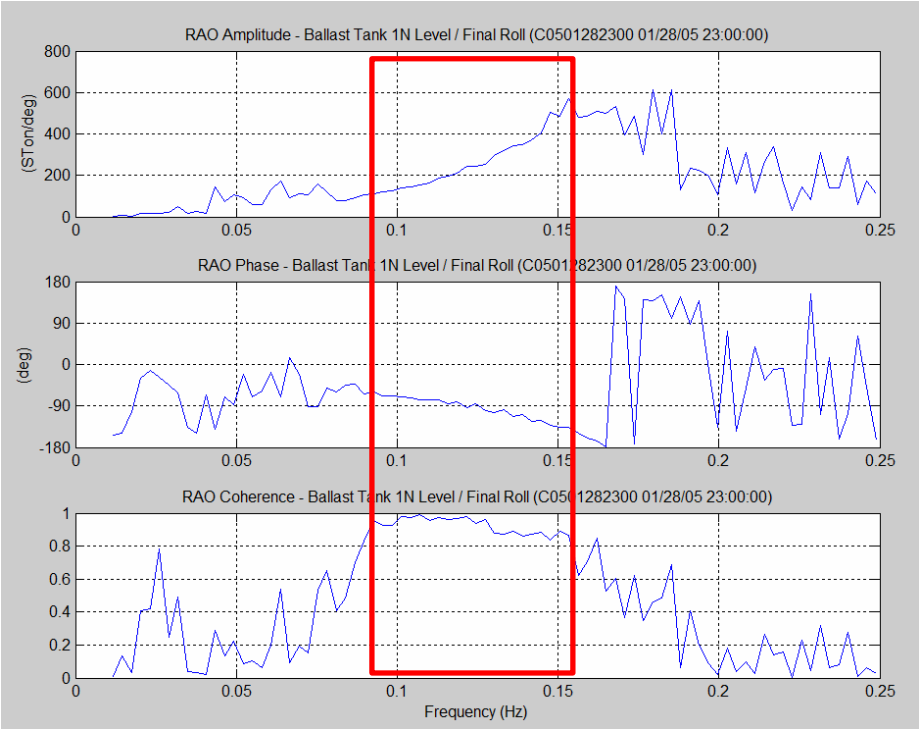

Figure 15: Coherence between roll and liquid level at wave frequences

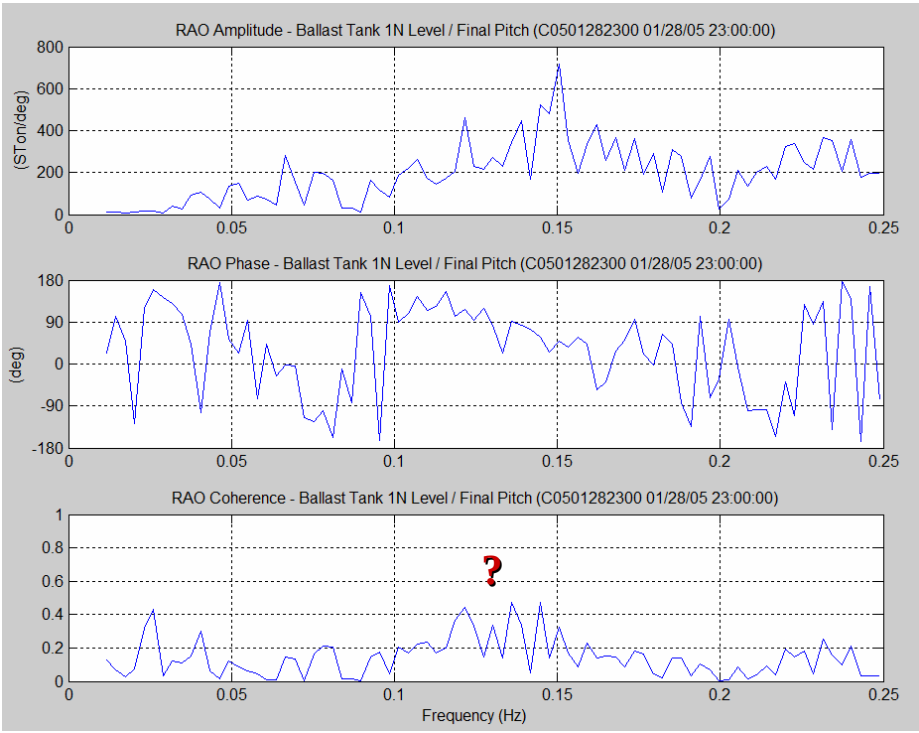

Figure 16: Coherence between pitch and liquid level at wave frequencies

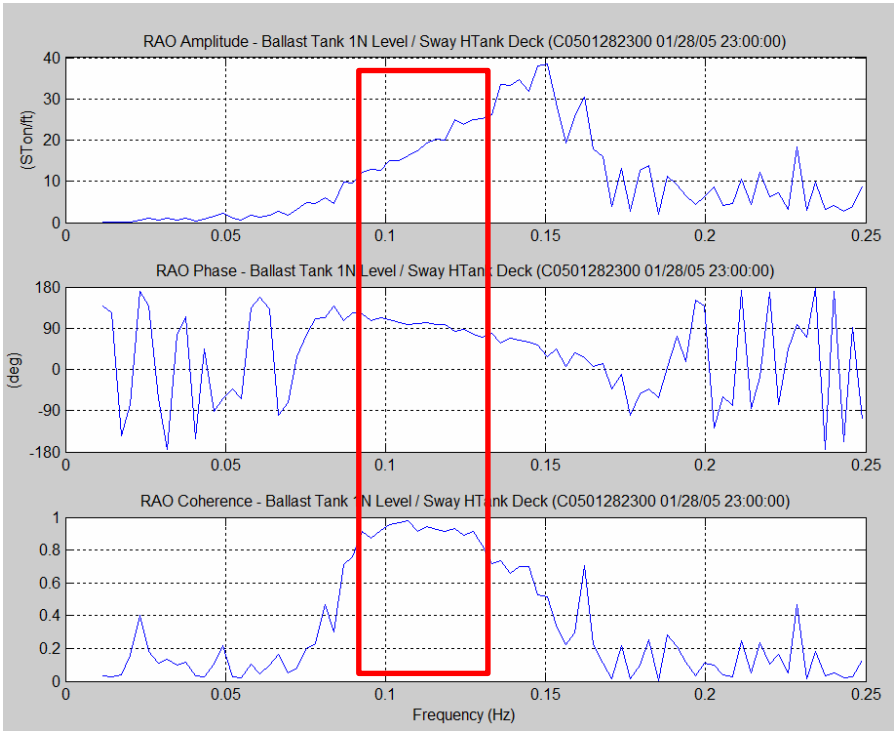

Figure 17: Coherence between sway and liquid level at wave frequences

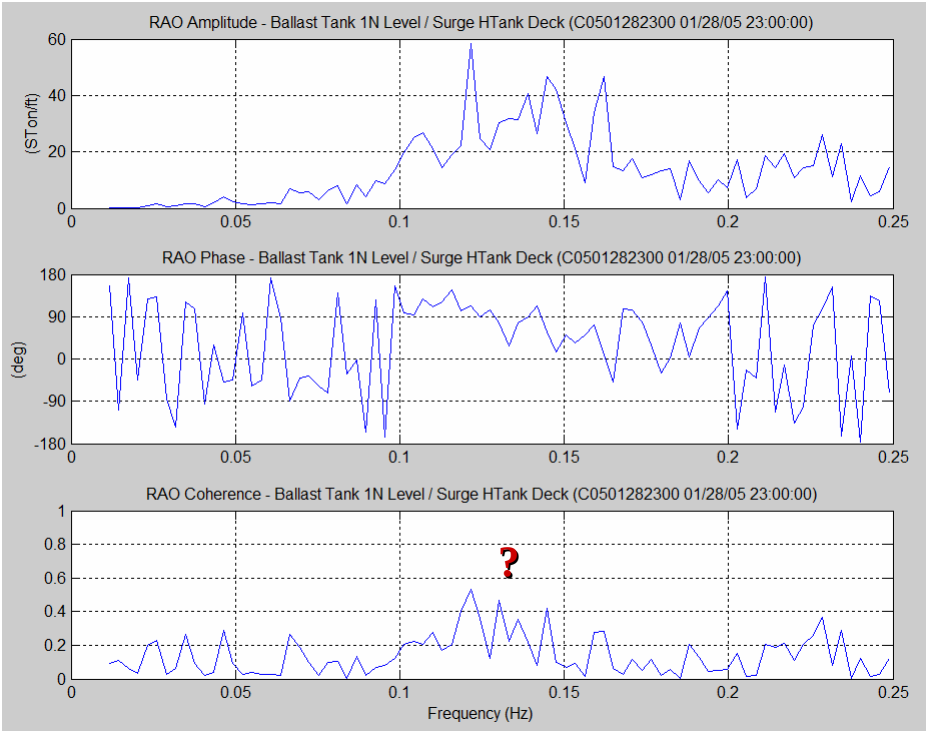

Figure 18: Coherence between surge and liquid level at wave frequences

A possibility for violent sloshing and splashing was also checked using the wavelet analysis method. This method differs from the coherence analysis in that it can capture the changes not only in frequency but also in time domain. This means that if splashing or wave breaking occurs, the wavelet scalogram[2] will show a noticeable change in the scalogram pattern, which can be clearly seen as white lines in Figure 19 and Figure 20 for several events. The most significant "splash" happened around 300 seconds (time= index*sampling_rate=600*0.5sec=300sec, as indicated in Figure 19). The regularity of "splash" events can be also observed in the figures.

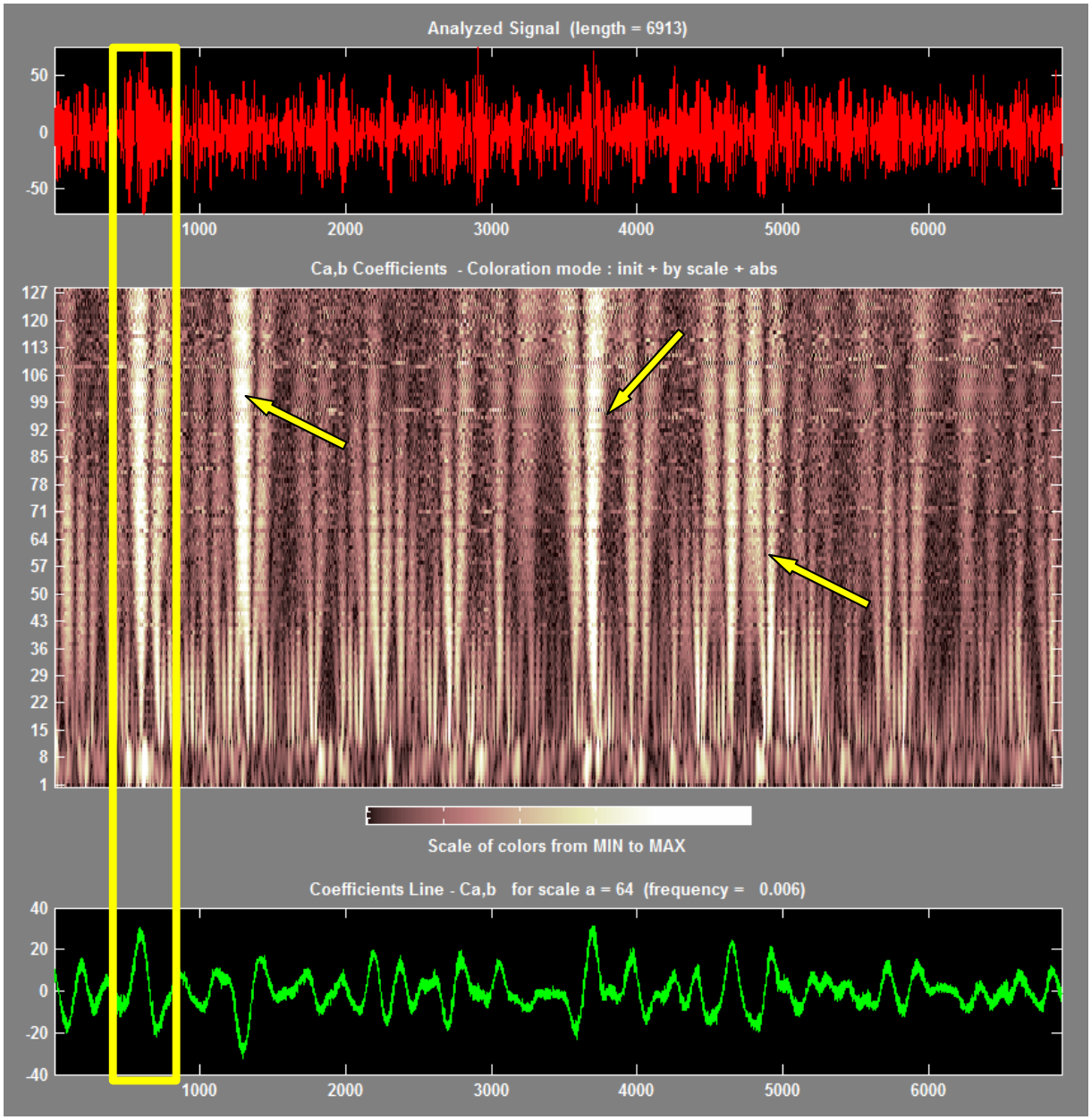

Figure 19: Wavelet scalogram of the liquid level measurement in the ballast tank on Medusa Spar

[2] Wavelet spectrogram called scalogram refers to a time-scale energy distribution defined as the square modulus of the wavelet coefficients. Scalogram is like spectrogram; however there is no trivial transition between scalogram and spectrogram.

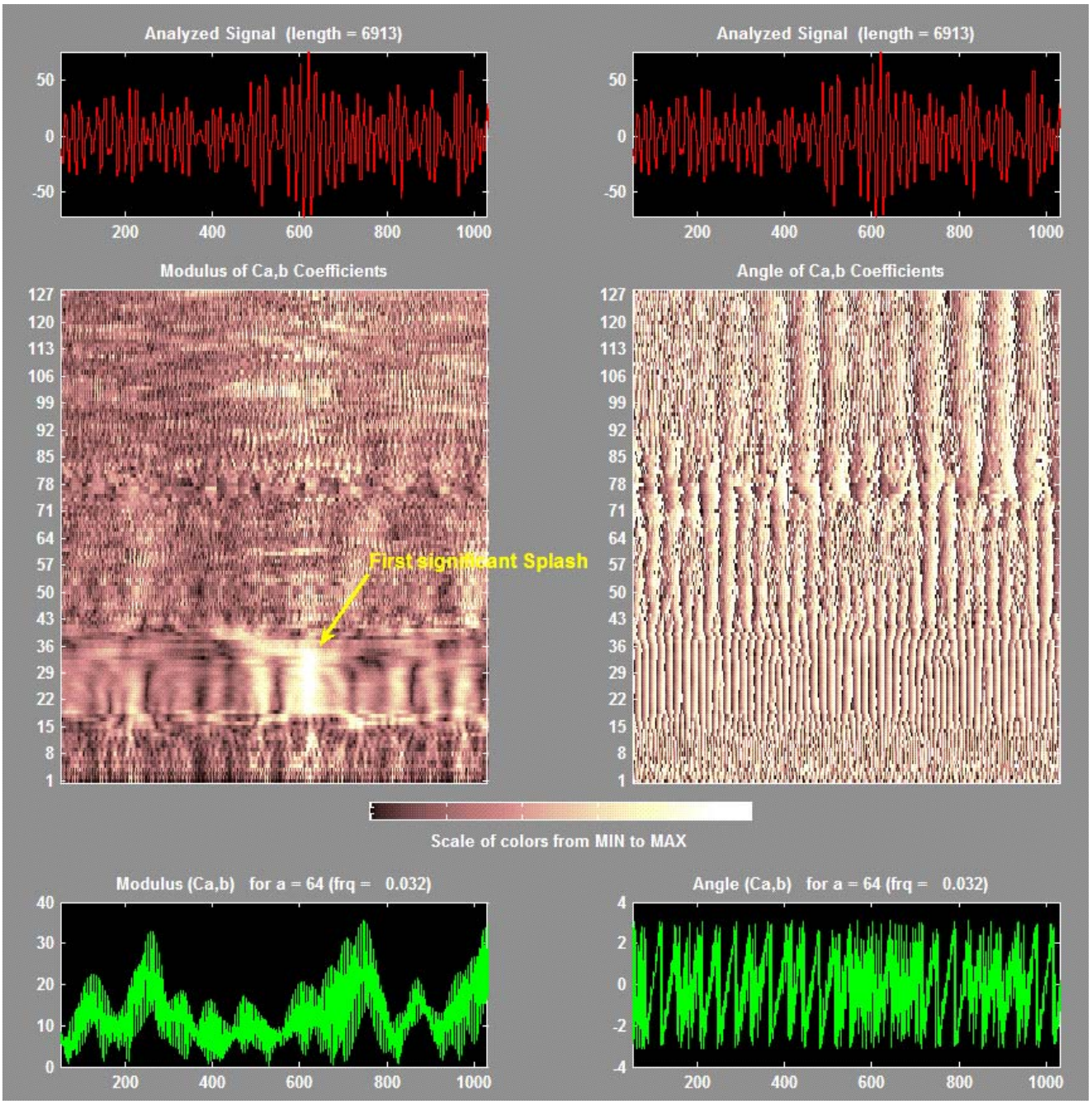

Figure 20: Modulus and phase of the wavelet transform of the liquid level measurement in the ballast tank on Medusa Spar.

6.3. Platforms Investigated

A total of three different platforms (i.e., two Spar platforms and one TLP platform), all located in the Gulf of Mexico, were considered in the CFD analysis:

- Medusa Spar
- Front Runner Spar
- Marlin TLP

6.4. Assessment Scenarios

A total of five simulations were carried out in the analysis, as presented in Table 2.

For Medusa Spar, a half-filled tank was considered and two different time intervals (of over 1000s) were investigated.

For Front Runner Spar, the same time interval was investigated with two different percentages filled (i.e. 50% and 25%).

For Marlin TLP, one simulation was carried out with a high filled level (i.e. 80%).

Table 2: Assessment Scenarios

Platform name	Run name	Simulation duration (s)	Time interval investigated		Initial water level above Deck 1	
			Start time (s)	End time (s)	(ft)	(m)
Medusa Spar	CaseF2	1233.65	1671.5	2905.15	28.2	8.61
	CaseF3	1025.65	71.5	1097.15	28.2	8.61
Front Runner Spar	CaseF10	650.5	71.5	722	35.8	10.912
	CaseF16	450	71.5	521.5	17.2	5.248
Marlin TLP	CaseF10	1125	35.75	1160.75	16.6	5.06

7. Numerical Analysis

The computational fluid dynamics analysis (CFD) was carried out using the CFX general-purpose suite of software tools. CFX has been widely validated by the software developer and by third parties, including BMT, for a variety of hydrodynamic and free surface applications.

7.1. Model Geometries

7.1.1. Ballast Tanks

Ballast tanks of offshore platforms (Spar or TLP) are very large structures partially filled with water. Typically, ballast tanks in Spar platforms are around 60 ft (~18m) in height and 1300 ft^2 (~120m^2) in cross-sectional area, whereas ballast tanks in TLP platforms are around 30 ft (~7m) in height and 1000 ft^2 (~90m^2) in cross-sectional area. They have very complex internal geometries and are made of many structural members, from large-scale objects (for example, ring frames and stringers) to small-scale features (for example, stiffeners). The complexity of the ballast tank geometry is presented in Figure 22 showing a picture of the ballast tanks of Front Runner Spar during construction.

7.1.2. Geometrical Simplifications

The models of the ballast tanks considered in the analysis were constructed based on engineering drawings supplied to BMT. Examples of engineering drawings used to build the models are presented in Figure 23, Figure 24 and Figure 25.

The models were simplified to neglect small-scale geometrical features judged to have negligible influence on the free surface motion. For example, stiffeners or very small access holes were not included in the models.

All models included the following main structural members, constructed using thin walls (i.e., without thickness):

- horizontal ring frames
- vertical deck girders
- vertical deck stringers
- horizontal struts
- large access holes

Perspective views of the models used for Medusa Spar, Front Runner Spar and Marlin TLP are presented in Figure 26, Figure 27 and Figure 28 respectively.

7.2. CFD Models

7.2.1. Computational Meshes

The computational meshes were generated in the fluid domain bounded by the ballast tanks walls. Cells were concentrated in the interface region between the liquid water and the air (i.e., free surface) and around the horizontal ring frames.

For ***Medusa Spar***, the unstructured computational mesh comprised of 650,000 cells (mainly hexagonal but also tetrahedral elements). A fine mesh was located in the free surface region. Figure 21 and Figure 29 present a cut plane through the mesh used for Medusa Spar.

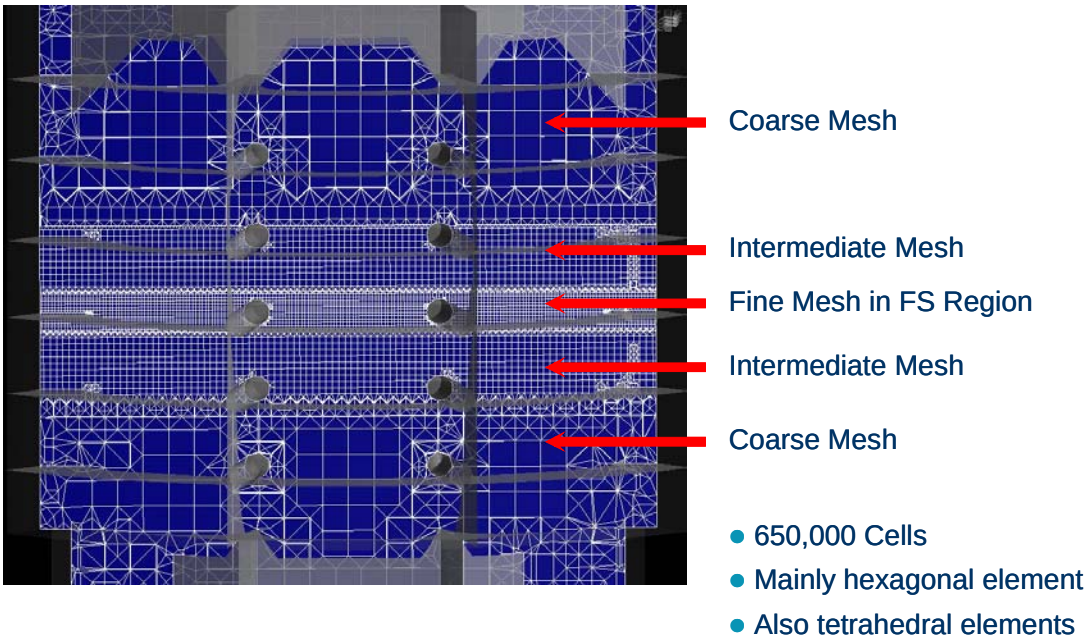

Figure 21: Computational mesh for the Medusa ballast tank

For ***Front Runner Spar***, the structured computational mesh comprised of 500,000 cells (mainly hexagonal but also prismatic elements) distributed into 84 layers. A fine mesh was located in the free surface region (e.g. 20 layers of 0.25 ft (0.075m) height). Figure 30 presents the mesh generated on the shell and the internal surfaces of Front Runner Spar.

For ***Marlin TLP***, the structured computational mesh comprised of 750,000 cells (mainly hexagonal but also prismatic elements) distributed into 110 layers. A fine mesh was located in the free surface region (e.g. 52 layers of 0.1 ft (0.033m) height. Figure 31 presents the mesh generated on the shell and the internal surfaces of Marlin TLP.

7.2.2. Numerical Models

7.2.2.1. Volume of Fluid (VOF) Model

Due to the presence of a distinct and well-defined interface between the two immiscible phases (i.e., water and air), the standard Volume of Fluid (VOF) model (or Free Surface model) available in CFX was chosen for the analysis. In the VOF model, a single set of momentum equations is shared by the fluids and the volume fraction of each of the fluids in each computational cell is tracked throughout the domain. An enhanced compression level was also used to improve the interface sharpness. Surface tension was not considered in the models.

7.2.2.2. Turbulence Model

The two-equation K-ε turbulence model was employed in the CFD simulations with standard coefficients. The K-ε turbulence model is widely used for applications in the offshore industry and is generally suitable for hydrodynamic analysis.

7.2.2.3. Heat Transfer Model

No heat transfer effects were modeled in the simulations.

7.2.3. Boundary Conditions

The surfaces of the ballast tanks (i.e., shells and internal structures) were modeled as smooth walls (i.e., no roughness) with a no-slip condition (u, v, w = 0). Six degree of freedom motions were imposed on the ballast tanks walls using displacement time histories provided to BMT (see Section 8). Therefore, no feedback due the fluid motion inside the tank was considered (i.e., forced displacements). The computational meshes were not deformed but moved solidly with the surfaces.

7.3. Fluid Properties

The sea water was modeled with a density of 1.989 slugs (1025 kg/m^3) and a viscosity of 1.12 x10^{-5} ft^2/s (1.04 x10^{-6} m^2/s).

The air was modeled with a density of 0.0025 slugs (1.284 kg/m^3) and a viscosity of 1.92x10^{-4} ft^2/s (1.39 x10^{-5} m^2/s).

7.4. Computational Requirements

7.4.1. Time Stepping

To achieve good convergence, the time steps used for the simulations needed to satisfy some specific requirements based on a (length/velocity) scale. Therefore, very small time steps (of the order of 1s) in comparison with the time domain to be simulated (of the order of 1000s) were used for the simulations.

7.4.2. Computational Time

Due to the small time steps used for the simulations and the complex geometry of the tanks (i.e., see Figure 29, Figure 30, and Figure 31), a couple of weeks were required to carry out a long simulation of more 1000s.

Figure 22: Picture of Front Runner Spar during construction

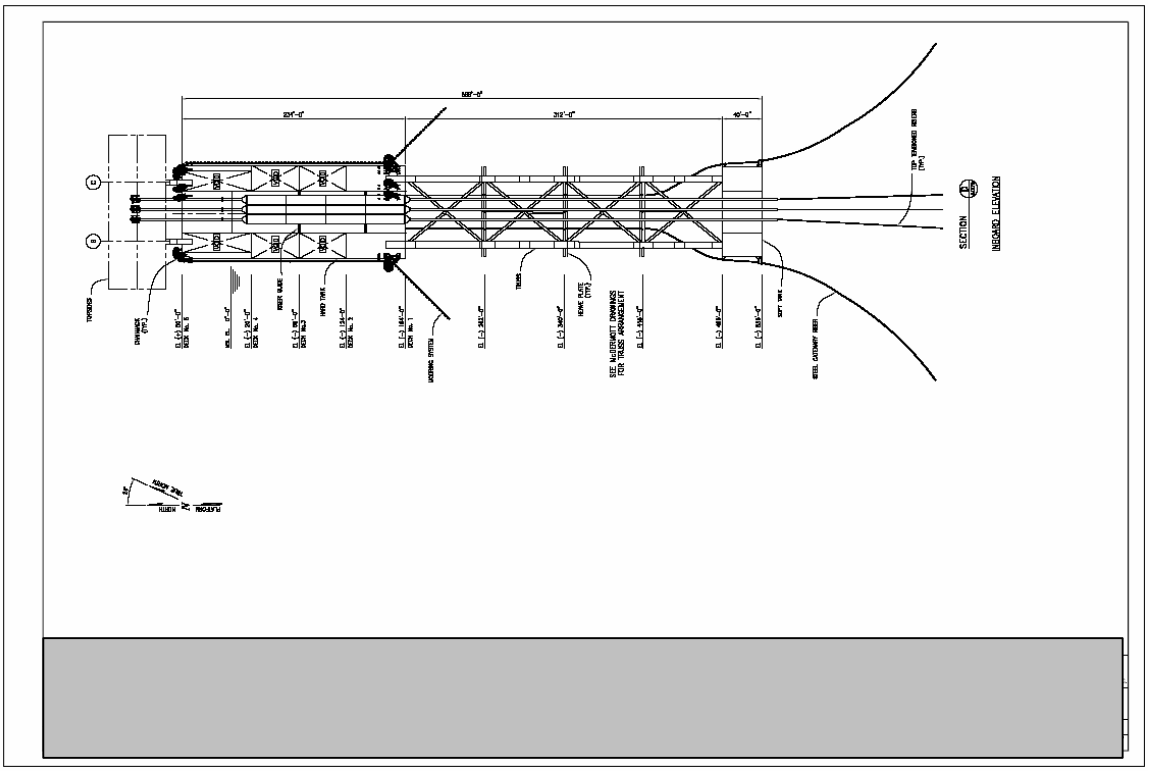

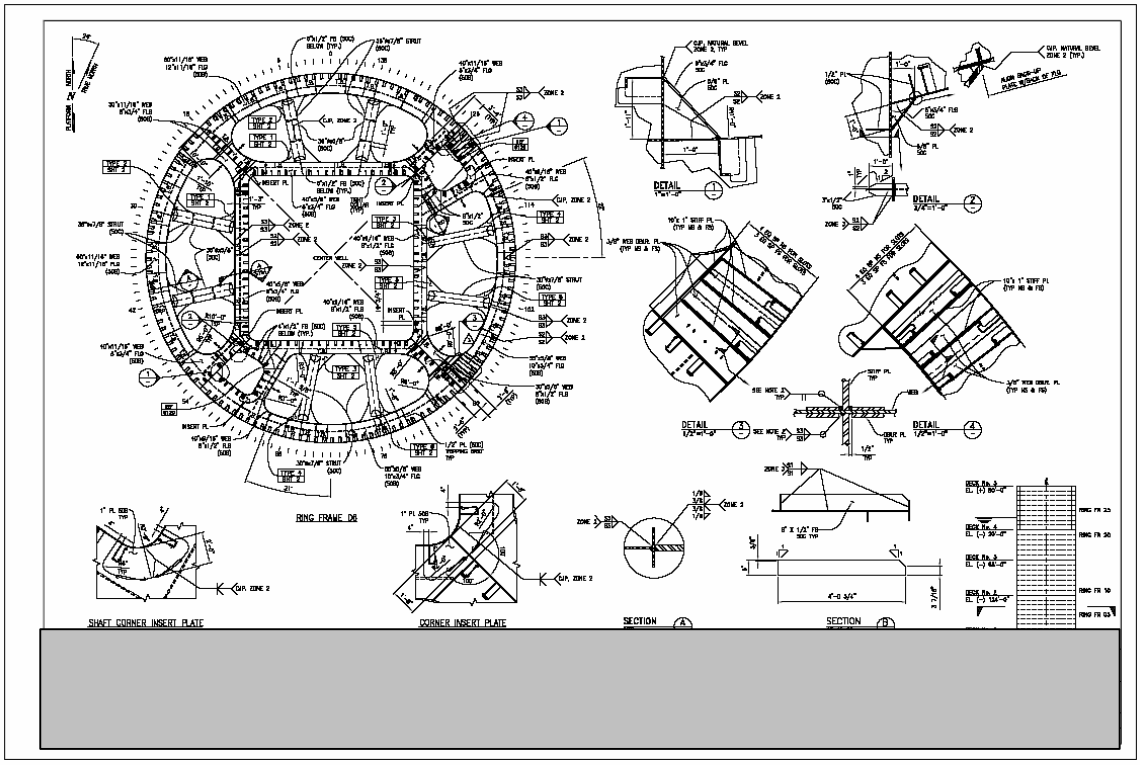

Figure 23: Examples of engineering drawings for Medusa Spar

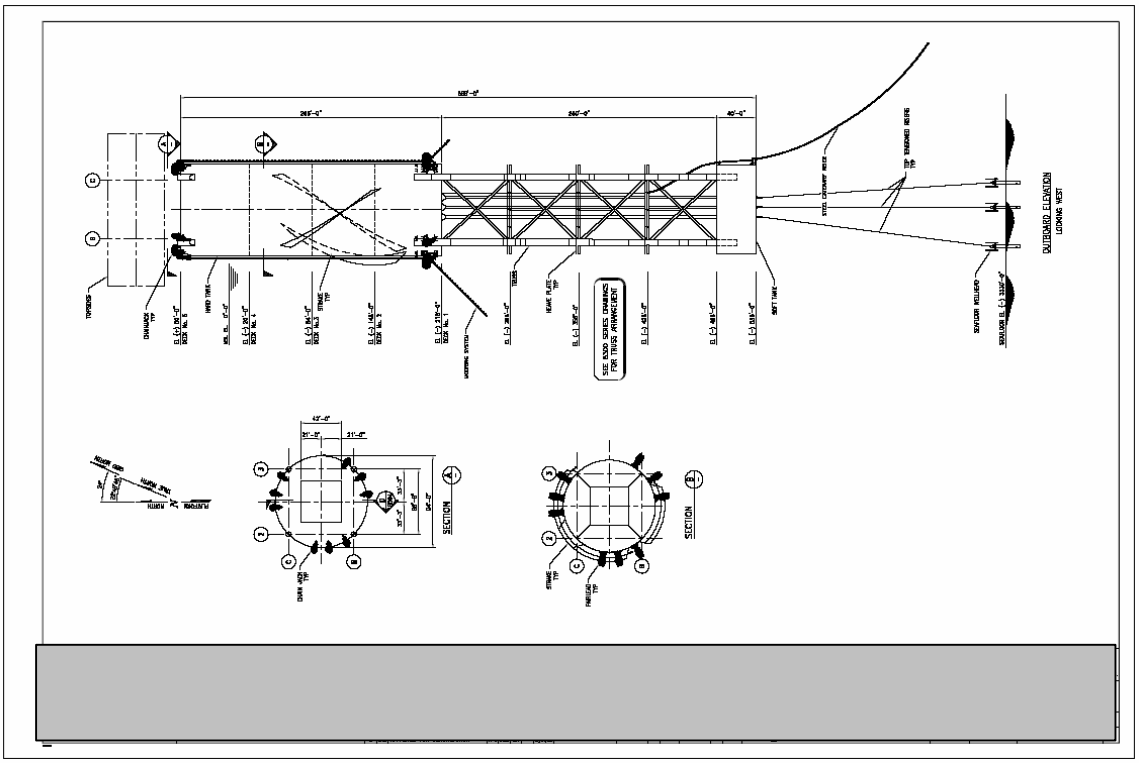

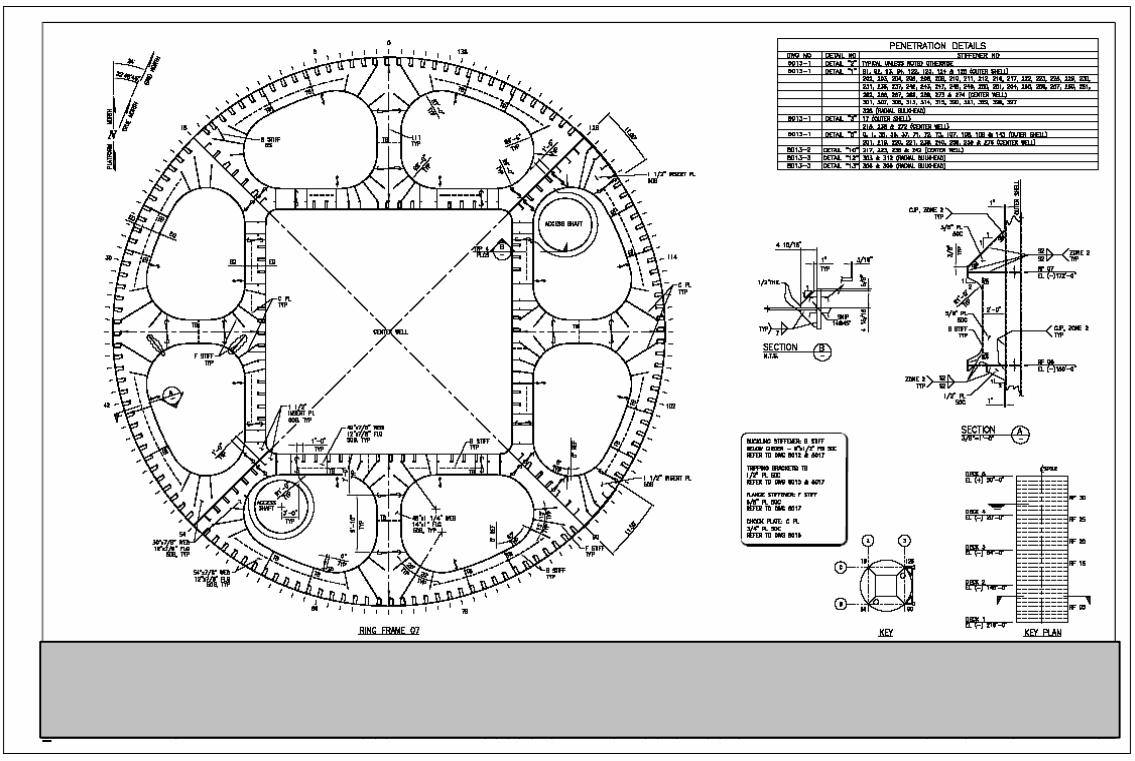

Figure 24: Examples of engineering drawings for Front Runner Spar

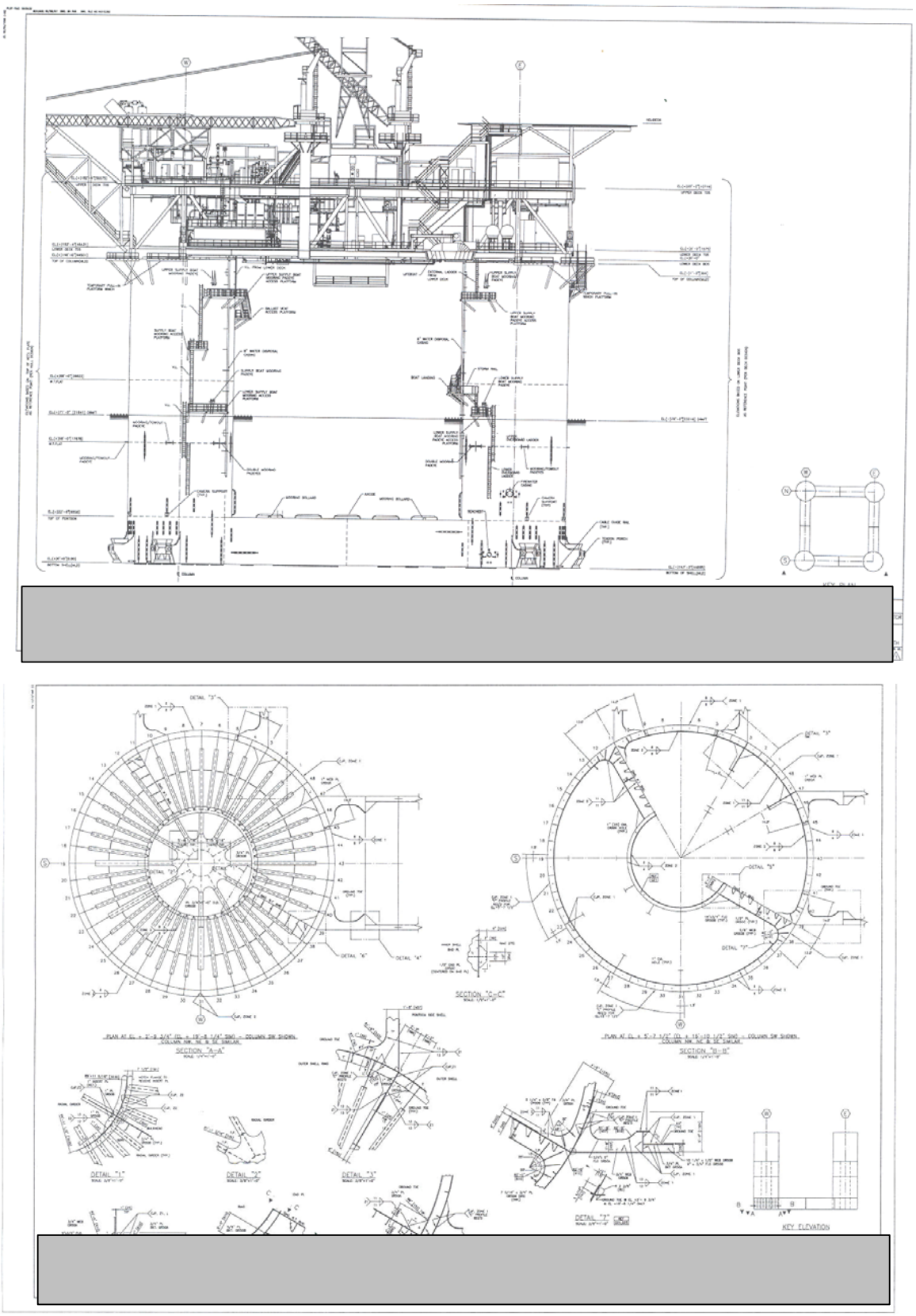

Figure 25: Examples of engineering drawings for Marlin TLP

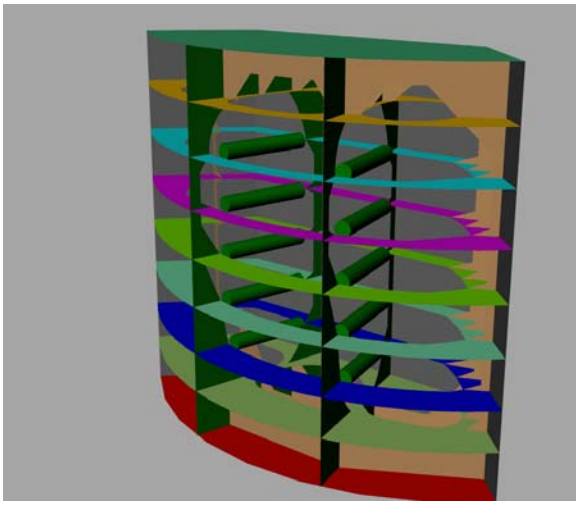

Vertical deck stringers

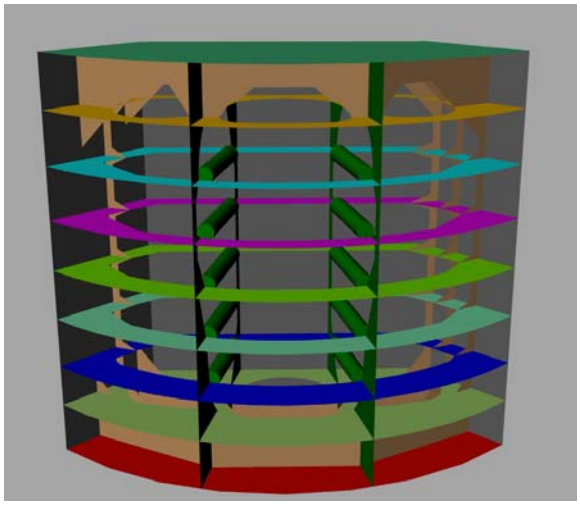

Horizontal ring frames

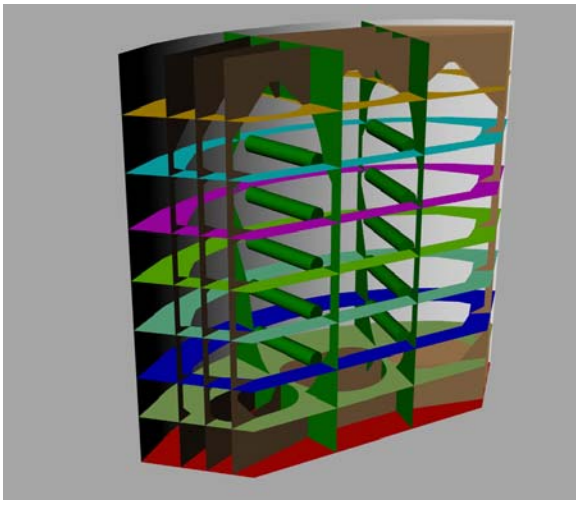

Horizontal struts

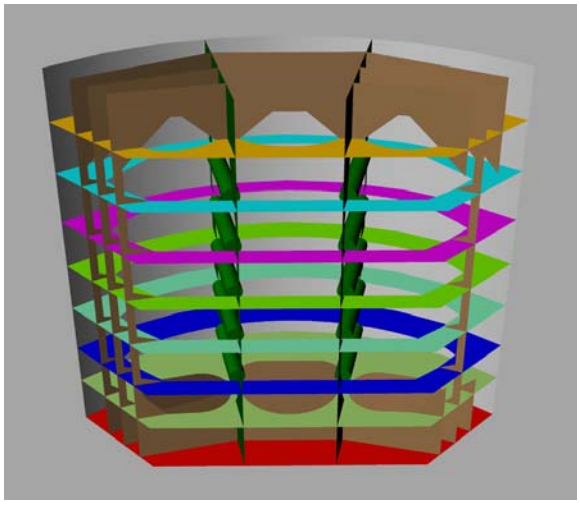

Vertical deck girders

Figure 26: CAD model for Medusa Spar

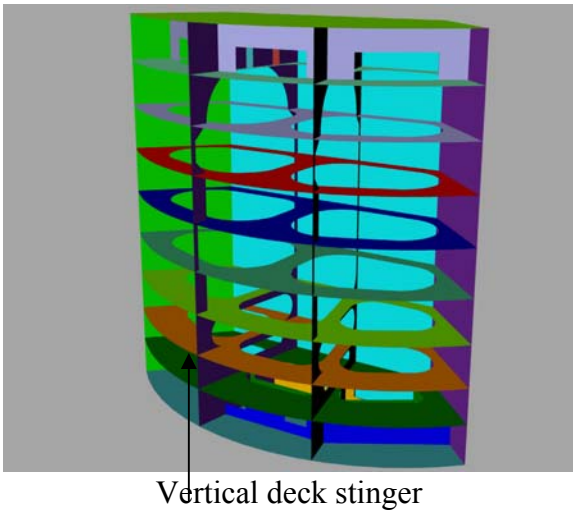

Figure 27: CAD model for Front Runner Spar

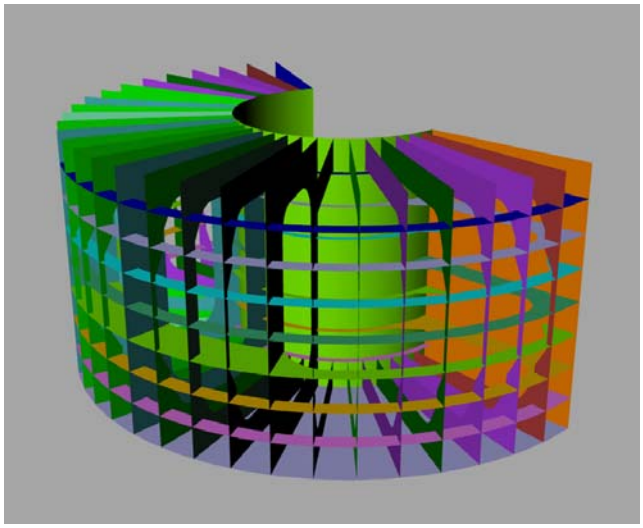

Horizontal ring frames

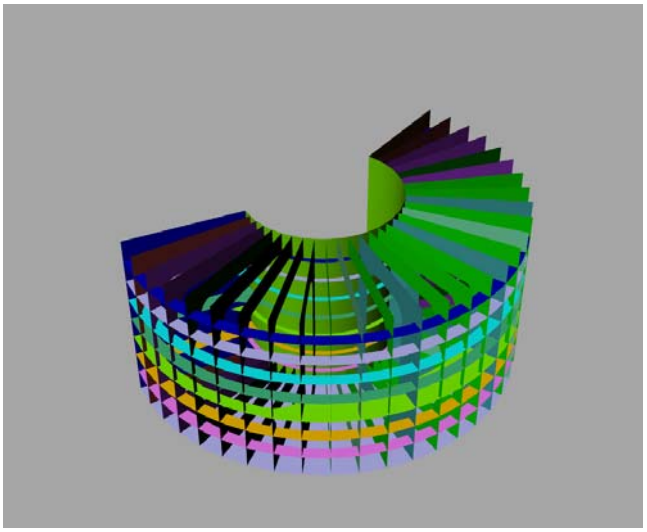

Vertical ring frames

Figure 28: CAD model for Marlin TLP

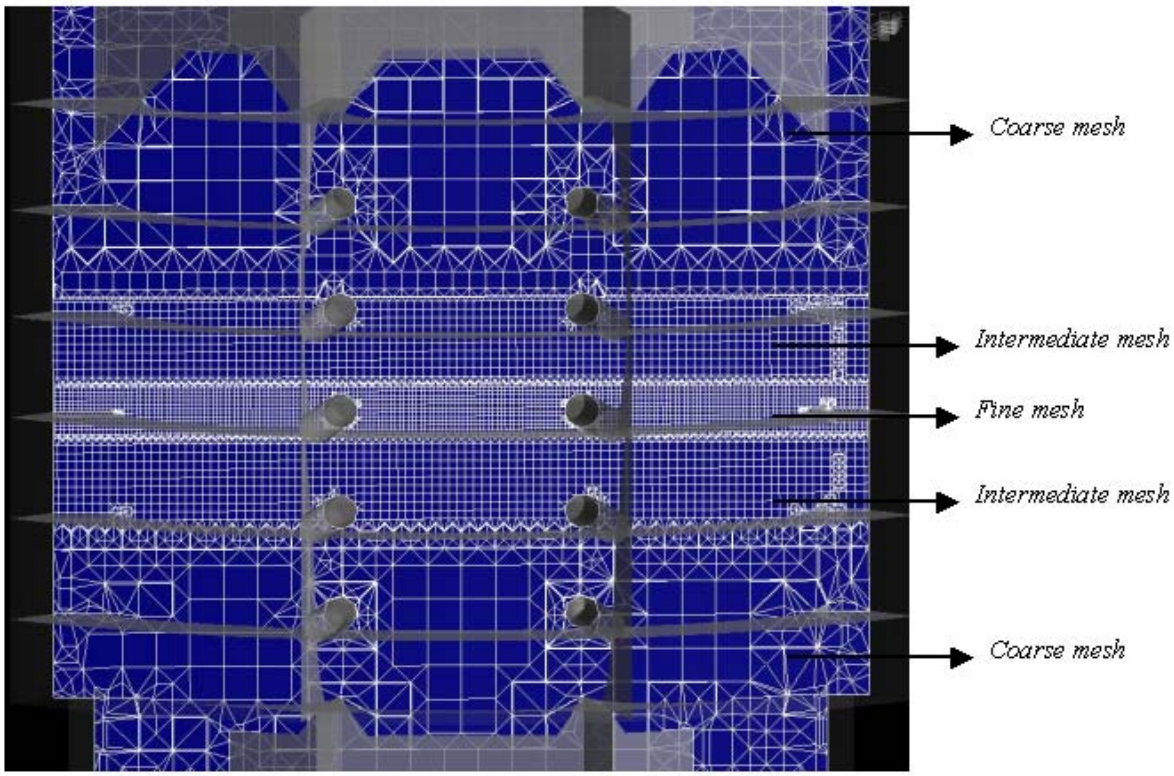

Figure 29: Computational mesh for Medusa Spar

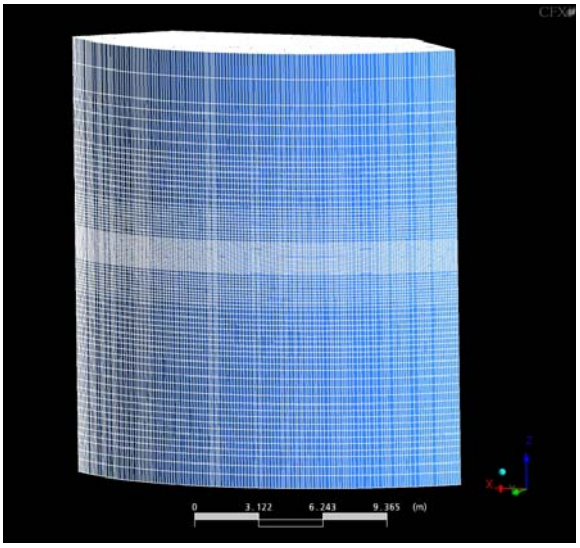

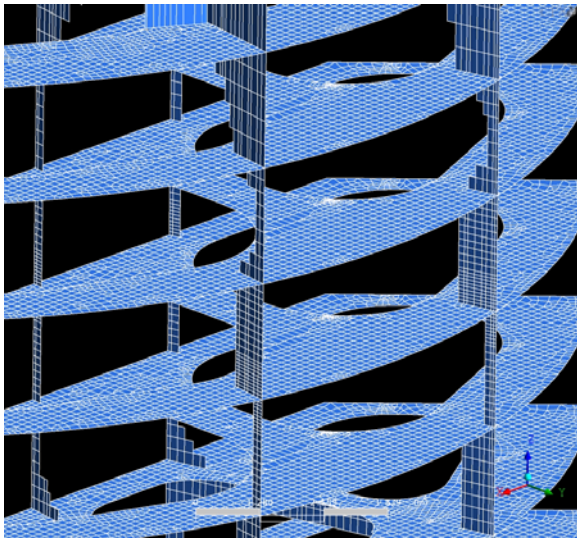

Fine mesh in free surface region

Figure 30: Computational mesh for Front Runner Spar

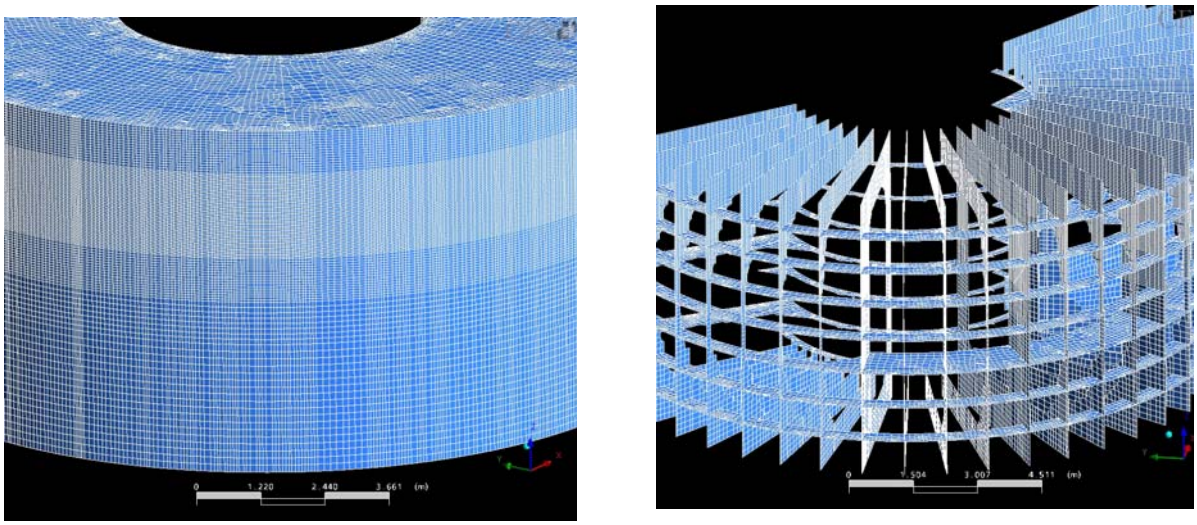

Fine mesh in free surface region

Figure 31: Computational mesh for Marlin TLP

8. Platform Motions

8.1. Time Histories

One of the four ballast tanks of each platform was selected for the analysis. Time histories of the tank motions were provided for 6 degrees of freedom for the Spar platforms and for 2 degrees of freedom (i.e., surge and sway) for the TLP platform. The reason for using only 2 degrees of freedom for the TLP is lack of measurements for other motions, because the other motions are considered negligible as they have been significantly suppressed due to stiff tendons.
The motions of the ballast tanks were provided in the platform coordinate systems.

The platform motions were defined as follows:

- Linear displacements:
  - X: positive surge towards platform North (platform bow)
  - Y: positive sway towards platform West (platform portside)
  - Z: positive heave upwards (against gravity)
- Angular displacements:
  - Around +X axis: positive roll (portside up)
  - Around +Y axis: positive pitch (bow down)
  - Around +Z axis: positive yaw (counter-clockwise when standing on the platform)

Time histories of more than 1 hour (with a sample time of 0.25s for the Spar platforms and 0.5s for the TLP platform) were used in the analysis.

Figure 32, Figure 33 and Figure 34 presents the time histories used in the analysis for Medusa Spar, Front Runner Spar and Marlin TLP respectively.

For Medusa Spar, large displacements were observed for the surge and sway motions (maximum displacement amplitudes of 24ft (7.3 m) and 42ft (12.8) respectively) whereas they were very small for the heave motion (maximum displacement amplitude of 0.9ft (0.3m). Motions due to roll, pitch and yaw were of the same order with maximum displacement amplitudes of 1.1deg, 0.5deg and 0.5deg respectively.

For Front Runner Spar, large displacements were observed for the surge and sway motions (maximum displacement amplitudes of 39ft (11.9m) and 32ft (9.7m) respectively) whereas they were very small for the heave motion (maximum displacement amplitude of 0.8ft (0.25m)). Motions due to roll, pitch and yaw were of the same order with maximum displacement amplitudes of 0.9deg, 0.5deg and 0.9deg respectively.

For Marlin TLP, large displacements were observed for the surge and sway motions (maximum displacement amplitudes of 24.5ft (7.5m) and 41.6ft (12.7m) respectively). Heave displacement and motions due to roll, pitch and yaw were not considered, as discussed above.

8.2. Spectral Analysis

8.2.1. Medusa Spar

The displacement spectra for Medusa Spar are presented in Figure 35 and three characteristic periods are identified:

- the natural wave period (around 9-10s)
- the platform natural periods of the ballast tank for surge and sway (around 50s)
- the platform natural periods of the ballast tank for roll, pitch and yaw (around 40s)

8.2.2. Front Runner Spar

The displacement spectra for Front Runner Spar are presented in Figure 36 and four characteristic periods are identified:

- the natural wave period (around 9-10s)
- the platform natural periods of the ballast tank for surge and sway (around 100s)
- the platform natural periods of the ballast tank for heave (around 60s)
- the platform natural periods of the ballast tank for roll, pitch and yaw (around 45s)

8.2.3. Marlin TLP

The displacement spectra for Marlin TLP are presented in Figure 37 and natural periods of the ballast tank of around 55s for both the surge and sway are identified.

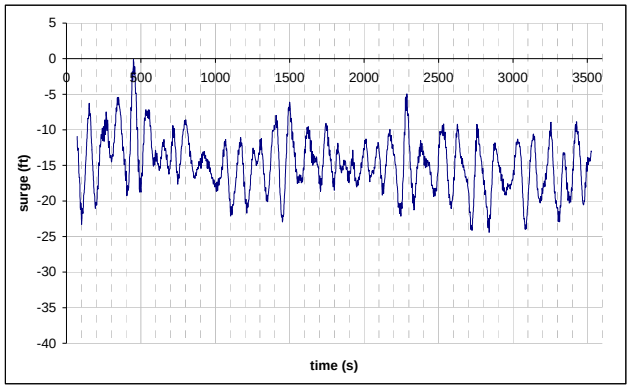

Surge displacement (in feet)

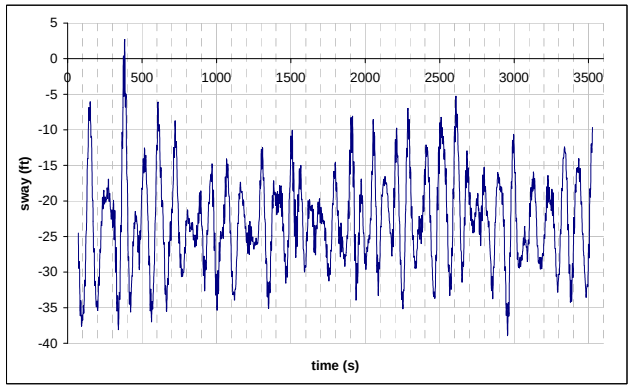

Sway displacement (in feet)

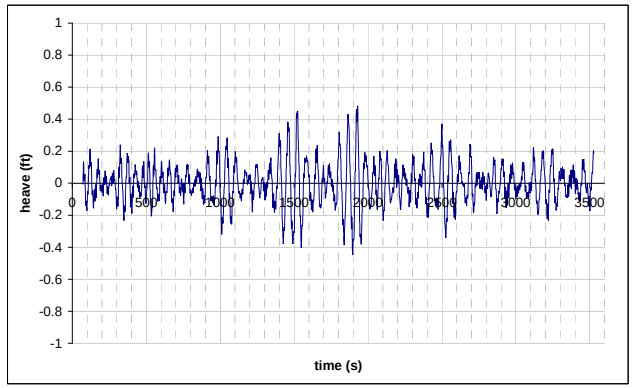

Heave displacement (in feet)

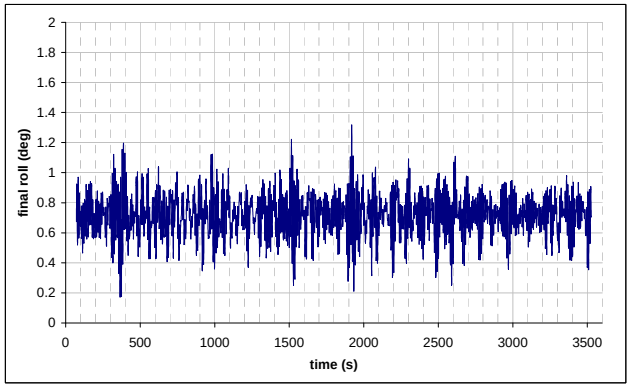

Roll displacement (in degree)

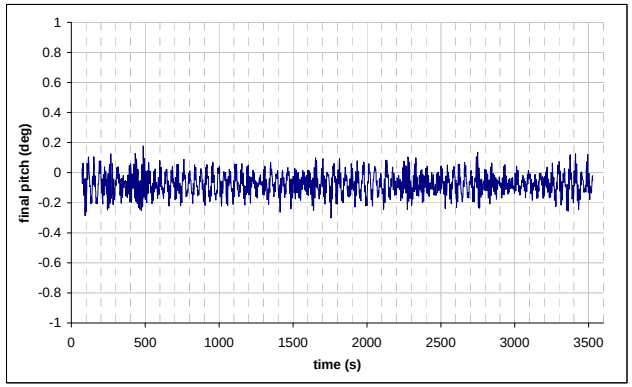

Pitch displacement (in degree)

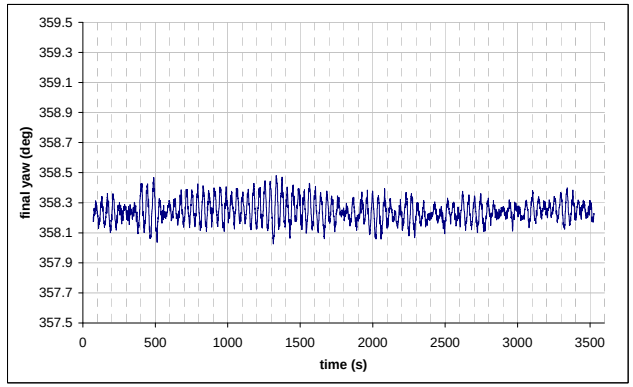

Yaw displacement (in degree)

Figure 32: Motion time histories for Medusa Spar

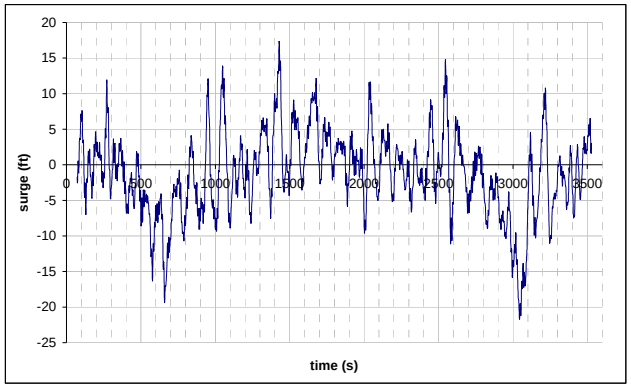

Surge displacement (in feet)

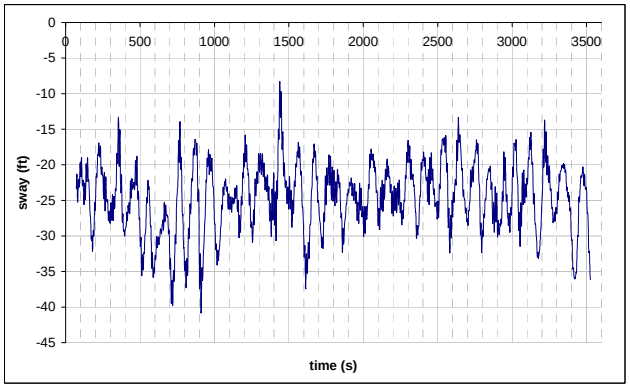

Sway displacement (in feet)

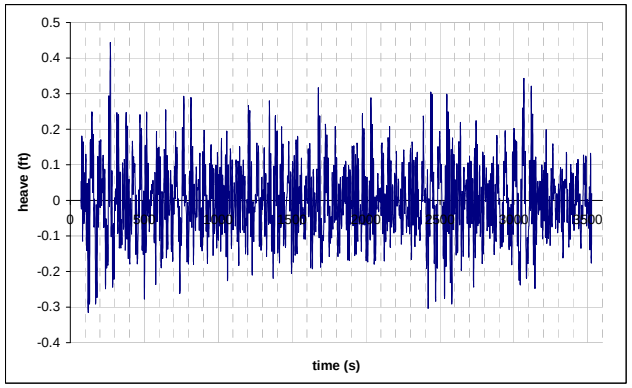

Heave displacement (in feet)

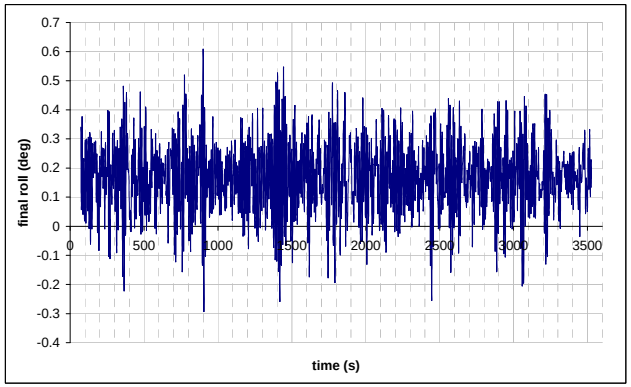

Roll displacement (in degree)

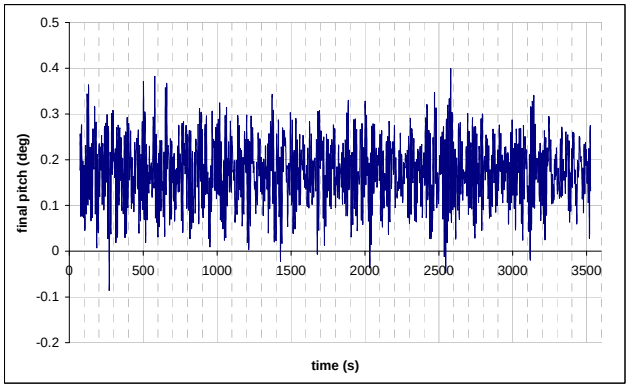

Pitch displacement (in degree)

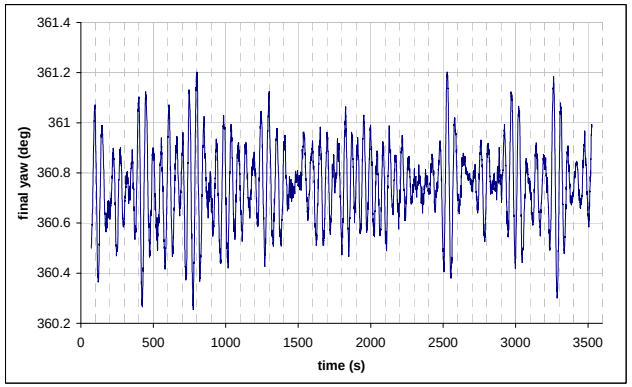

Yaw displacement (in degree)

Figure 33: Motion time histories for Front Runner Spar

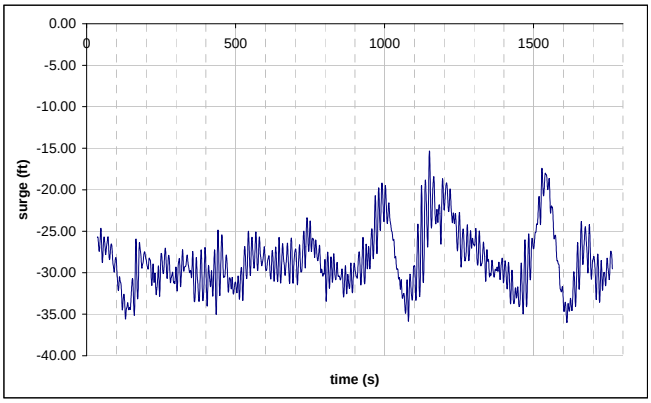

Surge displacement (in feet)

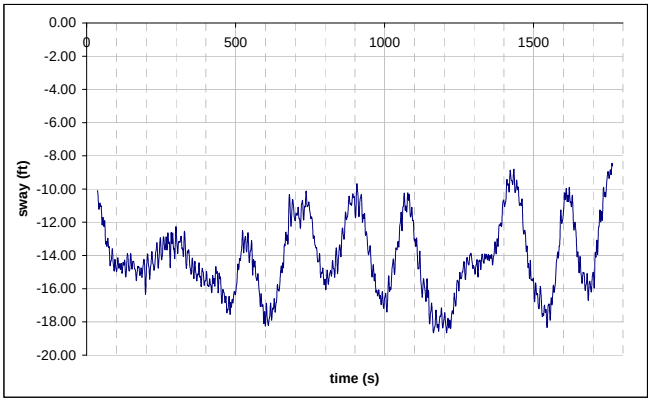

Sway displacement (in feet)

Figure 34: Motion time histories for Marlin TLP

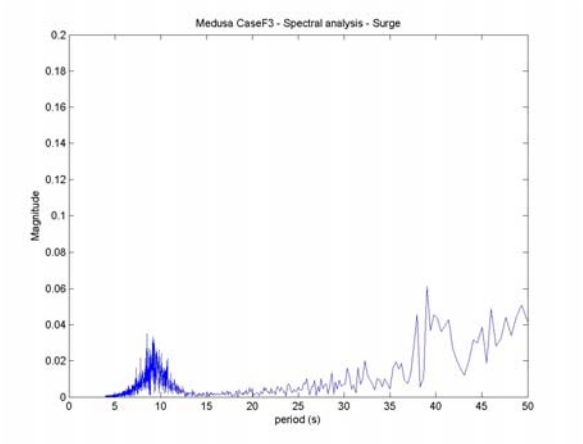

Surge displacement spectrum

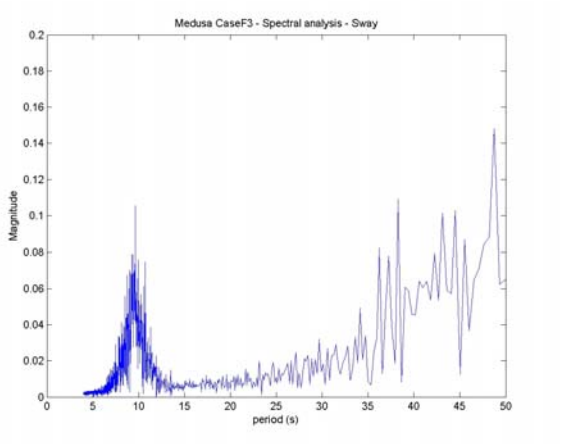

Sway displacement spectrum

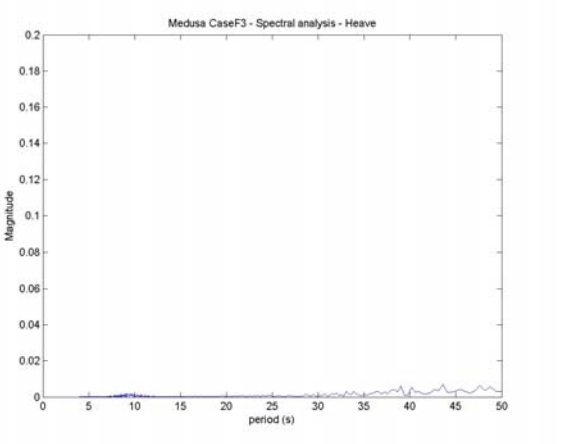

Heave displacement spectrum

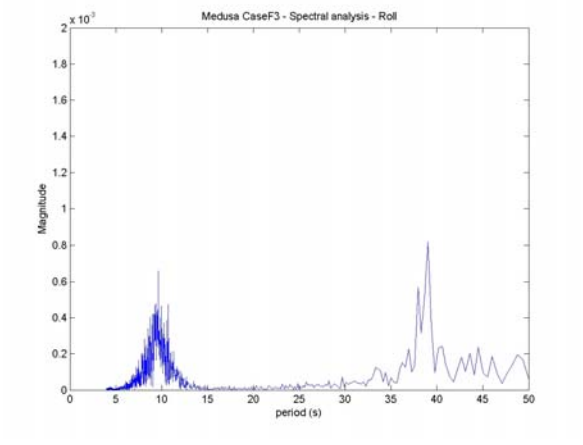

Roll displacement spectrum

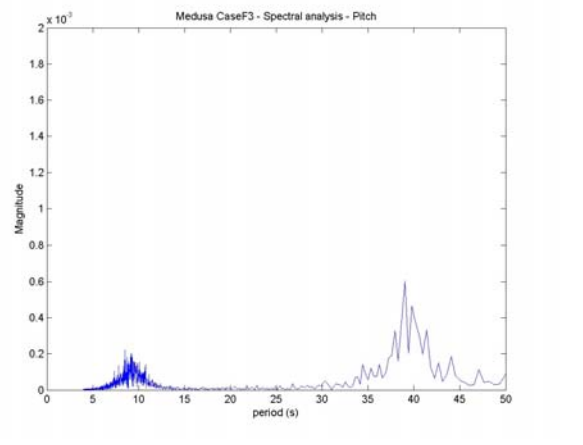

Pitch displacement spectrum

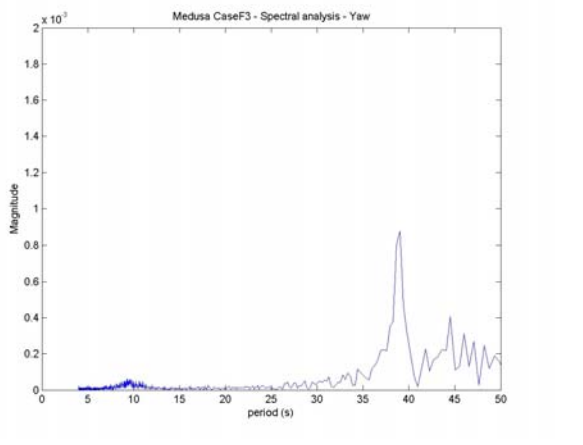

Yaw displacement spectrum

Figure 35: Motion spectra for Medusa Spar

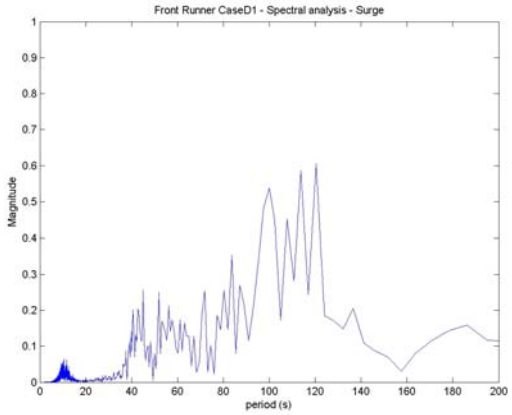

Surge displacement spectrum

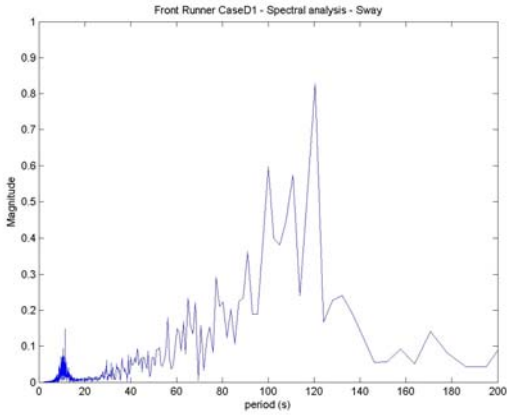

Sway displacement spectrum

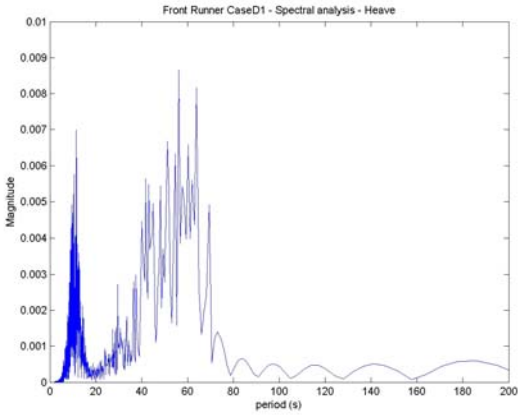

Heave displacement spectrum

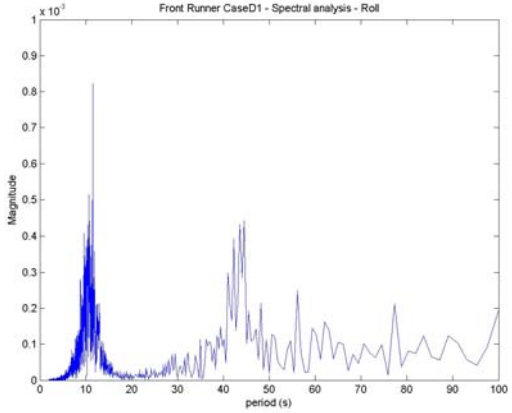

Roll displacement spectrum

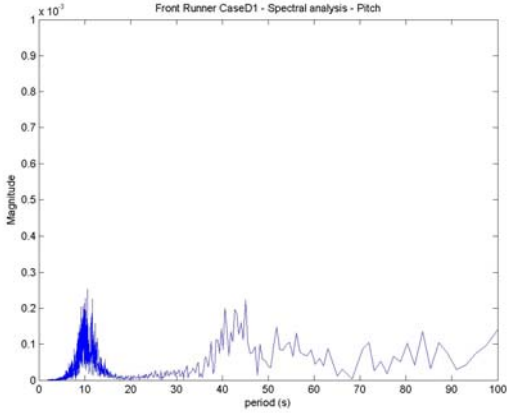

Pitch displacement spectrum

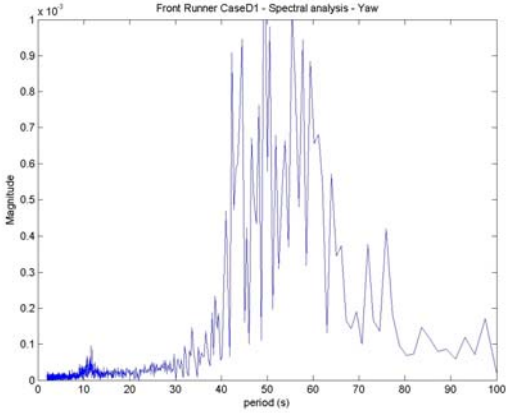

Yaw displacement spectrum

Figure 36: Motion spectra for Front Runner Spar

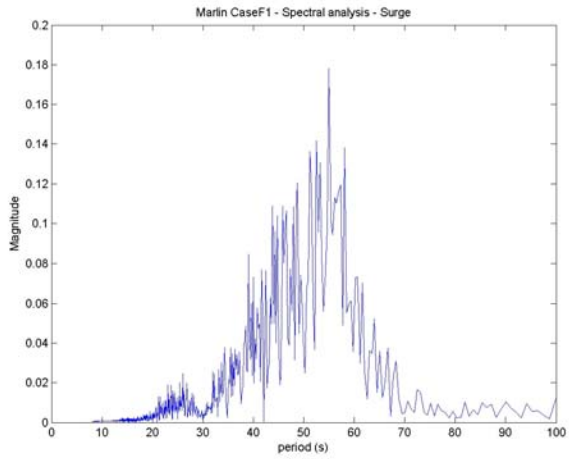

Surge displacement spectrum

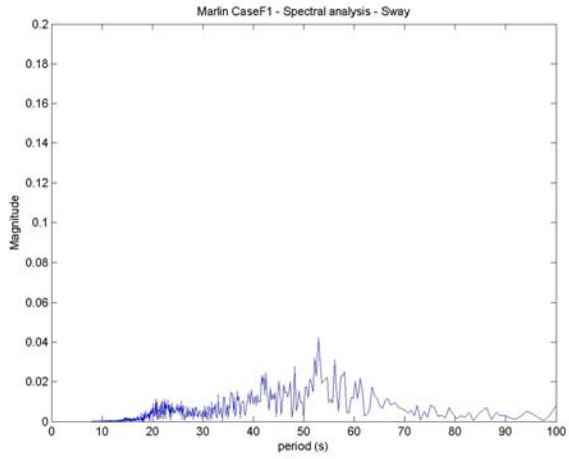

Sway displacement spectrum

Figure 37: Motion spectra for Marlin TLP

9. CFD Results

9.1. Validation of CFD method

The CFD method was validated first, before analyzing liquid motions in the tanks of other platforms. The validation of the CFD method was performed only using information provided for the:

- Ballast tank geometry and
- Platform six-degree of motions.

The measured liquid level was not provided up-front to the CFD modeler. Thus, the CFD calculation can be considered as a "blind" validation of the numerical model.

Only after the CFD calculations were done, the results for the measured water level in the ballast tank were disclosed and compared with the hindcast results, as shown in Figure 38. The results agree very well for a "blind" type of modeling.
The associated uncertainties with the CFD modeling are related to the

- Simplification of the ballast tank geometry and internal structural members used in the numerical model.
- Assumed amount of liquid in the tank (the amount of water in the tank was provided from the on-board tank advisory system)
- Measured 6DOF platform motions,
- Numerical limitations of the CFD program.

A very good preliminary agreement between the hindcast and the measured dynamic liquid levels provides a solid evidence that the CFD method and numerical settings are trustworthy and a similar approach can be used to perform similar calculations for other platforms.

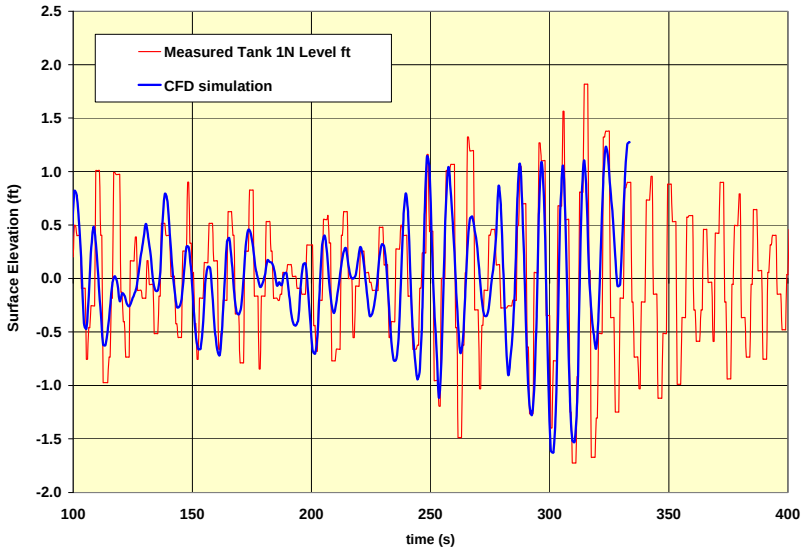

Figure 38: Measured and calculated liquid leve in a ballast tank of Medusa spar during the sloshing event between 310 and 320 sec)

9.2. Monitoring Point Locations

Evaluations of the effects of sloshing with respect to the liquid level sensor location and the amount of liquid (water) in the ballast tanks are performed at different monitoring points that cover the characteristics horizontal cross-sectional area of each of the tanks. More specific details are presented in the following paragraphs.

9.2.1. Medusa Spar

Pressure time histories were calculated at 5 different monitoring points, which were distributed on a same horizontal plane as shown in Figure 39. One point was located at the center of the ballast tank and the others were distributed close to the middle of each side of the tank. They were located approximately 8.2 ft (2.5m) below the initial water level (i.e. elevation of -164 ft (–50m)) in the platform coordinate system). Table 3 presents the coordinates of the monitoring points in the platform coordinate system.

9.2.2. Front Runner Spar

Pressure time histories were calculated at 5 different monitoring points, which were distributed on a same horizontal plane as shown in Figure 40. One point was located at the center of the ballast tank and the others were distributed close to the middle of each side of the tank. They were located approximately 10 ft (3m) below the initial water level (i.e. elevations of -190 ft (–58m) or -207ft (–63m) in the platform coordinate system). Table 4 presents the coordinates of the monitoring points in the platform coordinate system.

9.2.3. Marlin TLP

Pressure time histories were calculated at 5 different monitoring points, which were distributed on a same horizontal plane as shown in Figure 41. One point was located at the center of the ballast tank and the others were distributed close to the middle of each side of the tank. They were located approximately 2m below the initial water level (i.e., elevation of 10 ft (3m) in the platform coordinate system). Table 5 presents the coordinates of the monitoring points in the platform coordinate system.

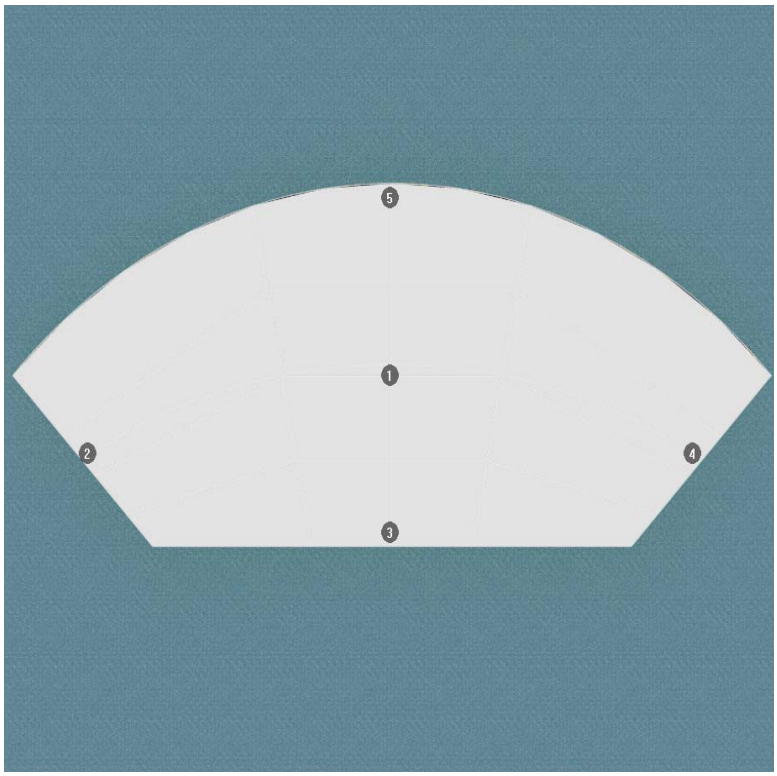

Figure 39: Monitoring points distribution for Medusa Spar – Plan view

Monitoring point number	Coordinates at initial time (in the platform coordinate system)					
	X_0		Y_0		Z_0	
	(ft)	(m)	(ft)	(m)	(ft)	(m)
1	33.23	10.13	0.00	0	-164 (*)	-50 (*)
2	27.67	8.435	26.49	8.074	-164 (*)	-50 (*)
3	22.00	6.706	0.00	0	-164 (*)	-50 (*)
4	27.67	8.435	-26.49	-8.074	-164 (*)	-50 (*)
5	46.00	14.021	0.00	0	-164 (*)	-50 (*)

(*): Z_0 = -50m corresponds to 2.5m below the initial water level

Table 3: Monitoring points coordinates for Medusa Spar

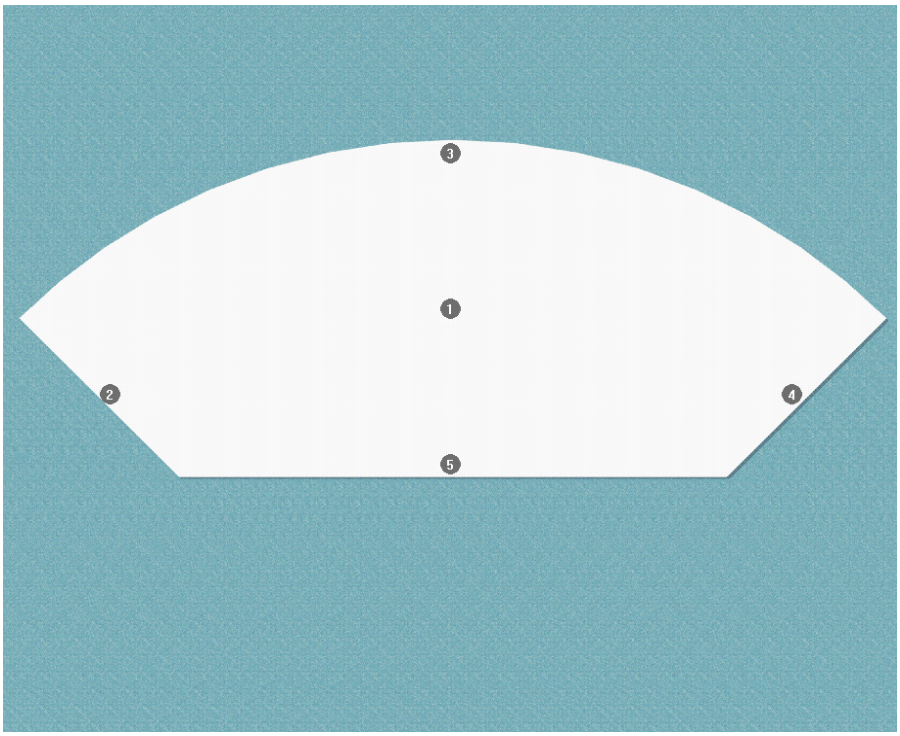

Figure 40: Monitoring points distribution for Front Runner Spar – Plan view

Monitoring point number	Coordinates at initial time (in the platform coordinate system)					
	X_0		Y_0		Z_0	
	(ft)	(m)	(ft)	(m)	(ft)	(m)
1	34.00	10.363	0.00	0	-190 (CaseF10) (*) -207 (CaseF16) (**)	-58 (CaseF10) (*) -63 (CaseF16) (**)
2	27.36	8.34	26.12	7.96	-190 (CaseF10) (*) -207 (CaseF16) (**)	-58 (CaseF10) (*) -63 (CaseF16) (**)
3	22.00	6.706	0.00	0	-190 (CaseF10) (*) -207 (CaseF16) (**)	-58 (CaseF10) (*) -63 (CaseF16) (**)
4	27.36	8.34	-26.12	-7.96	-190 (CaseF10) (*) -207 (CaseF16) (**)	-58 (CaseF10) (*) -63 (CaseF16) (**)
5	46.00	14.021	0.00	0	-190 (CaseF10) (*) -207 (CaseF16) (**)	-58 (CaseF10) (*) -63 (CaseF16) (**)

(*): Z_0 = -58m corresponds to 3m below the initial water level
(**): Z_0 = -63m corresponds to 3m below the initial water level

Table 4: Monitoring points coordinates for Front Runner Spar

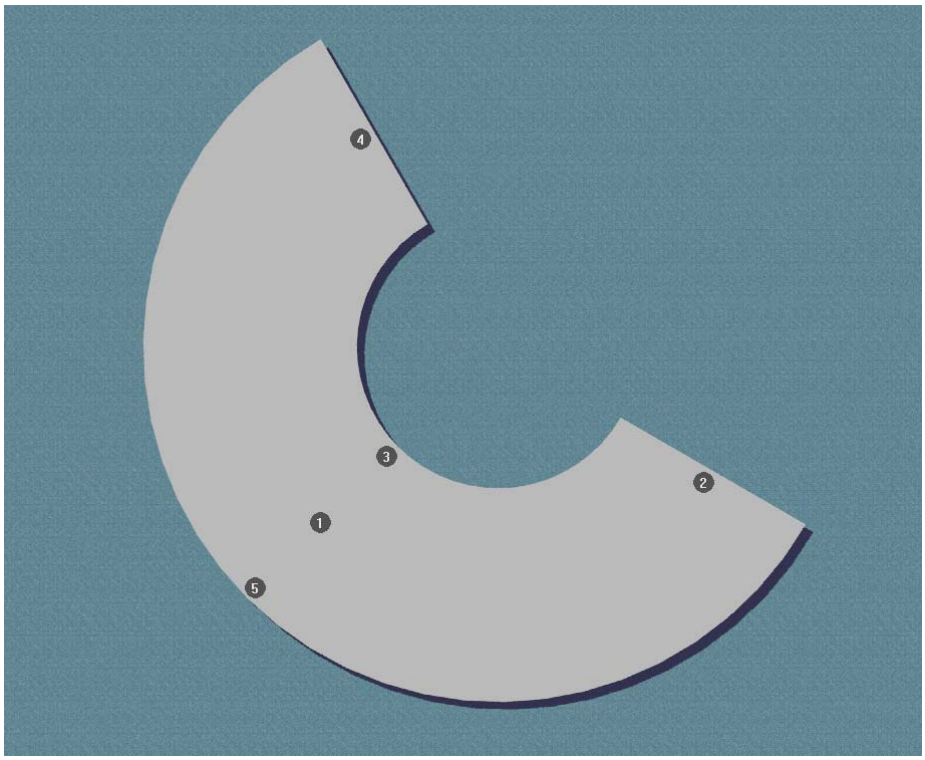

Figure 41: Monitoring points distribution for Marlin TLP – Plan view

Monitoring point number	Coordinates at initial time (in the platform coordinate system)					
	X_0		Y_0		Z_0	
	(ft)	(m)	(ft)	(m)	(ft)	(m)
1	-92.36	-28.15	92.36	28.15	9.8 (*)	3 (*)
2	-89.57	-27.30	65.38	19.93	9.8 (*)	3 (*)
3	-87.74	-26.74	87.74	26.74	9.8 (*)	3 (*)
4	-65.40	-19.93	89.56	27.30	9.8 (*)	3 (*)
5	-96.98	-29.56	96.98	29.56	9.8 (*)	3 (*)

(*): Z_0 = 3m corresponds to 2m below the initial water level

Table 5: Monitoring points coordinates for Marlin TLP

9.3. Pressure Time Histories

9.3.1. Medusa Spar

Pressure time histories are presented in Figure 42 for CaseF2 and Figure 44 for CaseF3. Significant free surface displacements were principally observed at monitoring points 2 and 4. At these two points, the free surface oscillated between a minimum elevation of -157.2 ft (-47.9m) and a maximum elevation of -154.5ft (-47.1m) (corresponding to an amplitude of 2.5 ft (0.8m), whereas at monitoring points 1, 3 and 5, an amplitude of less than 0.3ft (0.1m) was observed.

9.3.2. Front Runner Spar

Pressure time histories are presented in Figure 46 for CaseF10 and Figure 48 for CaseF16. Significant free surface displacements were observed at all monitoring points, except monitoring point 1.

9.3.3. Marlin TLP

Pressure time histories are presented in Figure 50 for CaseF10. Significant free surface displacements were observed at all monitoring points. At monitoring point 4, the free surface oscillated between a minimum elevation of 15.4ft (4.7m) and a maximum elevation of 17.7 ft (5.4m) (corresponding to an amplitude of 2.3ft (0.7m).

9.4. Pressure Spectra

9.4.1. Medusa Spar

Spectra of the pressure time histories are presented in Figure 43 for CaseF2 and Figure 45 for CaseF3. Two characteristic periods around 9-10s and around 40s for the free surface motions were observed. The principal response period was around 9-10s, showing a strong correlation with the wave period.

A typical comparisons between the free surface response periods and the surge and roll motion natural periods are shown later in **Error! Reference source not found.Error! Reference source not found.**.

9.4.2. Front Runner Spar

Spectra of the pressure time histories are presented in Figure 47 for CaseF10 and Figure 49 for CaseF16. The principal sloshing response period was around 9-10s, showing a strong correlation with the wave period.

9.4.3. Marlin TLP

Spectra of the pressure time histories are presented in Figure 51 for CaseF10. The principal response period was around 9-10s, which does not correspond to any of the natural periods observed for the surge and sway motions.

9.5. Effect of initial filled levels on liquid level motions in the ballast tank

The effect of initial filled levels on liquid level motions in tanks is studied using the ballast tank CFD model for Front Runner Spar. A comparison of the free surface displacements at the different monitoring points between CaseF10 and CaseF16 (i.e., different initial filled levels) is given in Figure 52.
The numerical simulations show that:

- The free surface response periods were not affected by change in initial filled level.
- At monitoring point 2, the amplitudes of the free surface displacement were larger for CaseF16 (amplitude of around 2ft (0.6m)) than for CaseF10 (amplitude of 1.4 ft (0.4m)). This is due to the presence of a horizontal ring frame very close to the initial free surface location in CaseF10, damping the free surface motion.

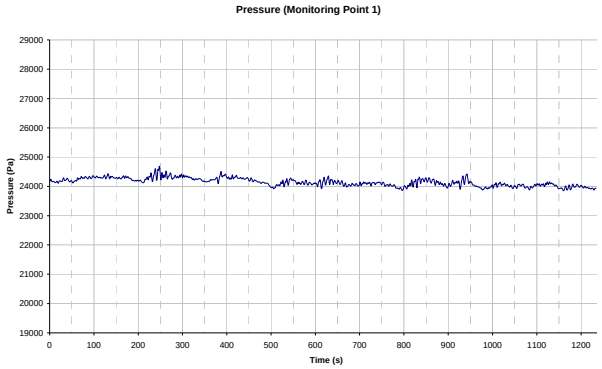

Monitoring point 1 – Pressure time histories

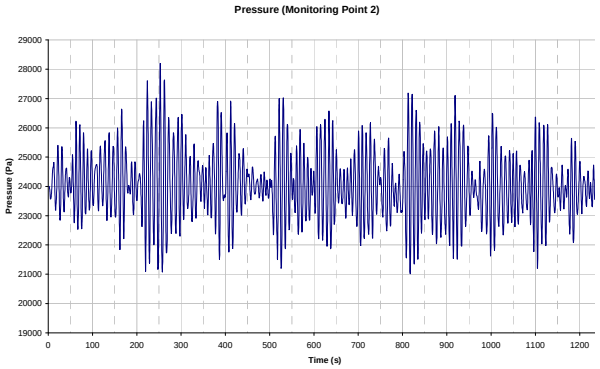

Monitoring point 2 – Pressure time histories

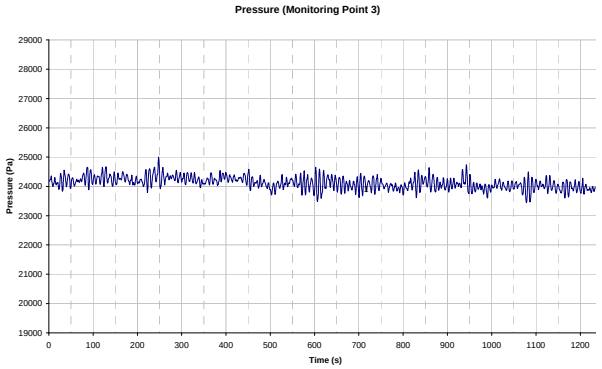

Monitoring point 3 – Pressure time histories

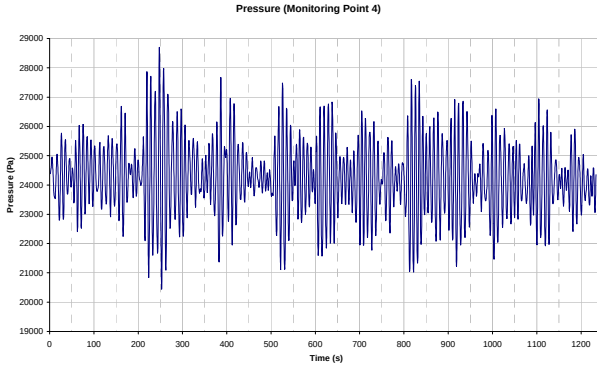

Monitoring point 4 – Pressure time histories

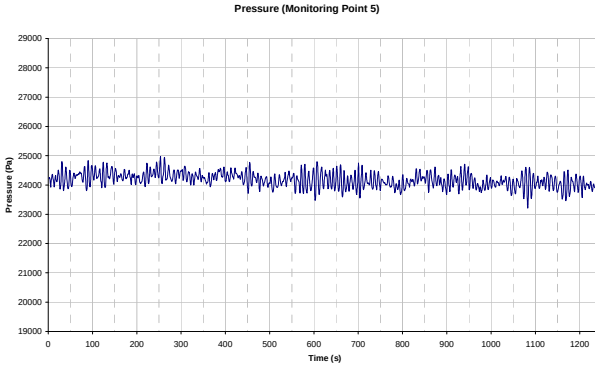

Monitoring point 5 – Pressure time histories

Figure 42: Pressure time histories – Medusa Spar – CaseF2

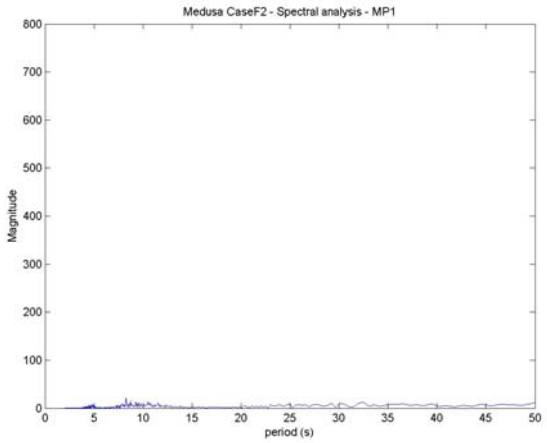

Monitoring point 1 – Spectrum

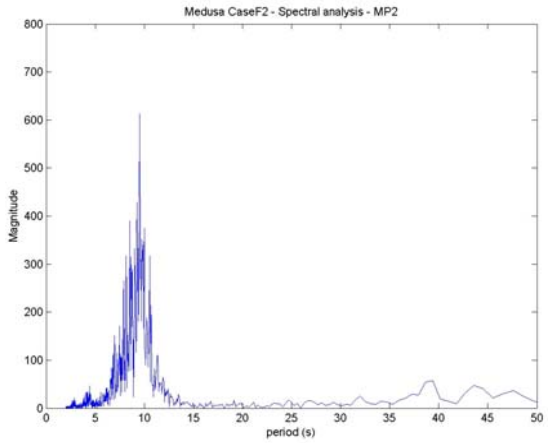

Monitoring point 2 – Spectrum

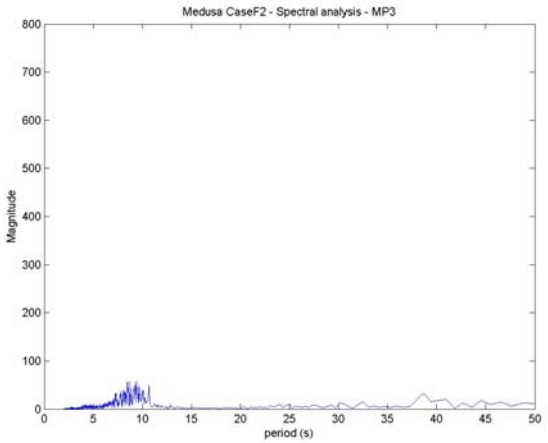

Monitoring point 3 – Spectrum

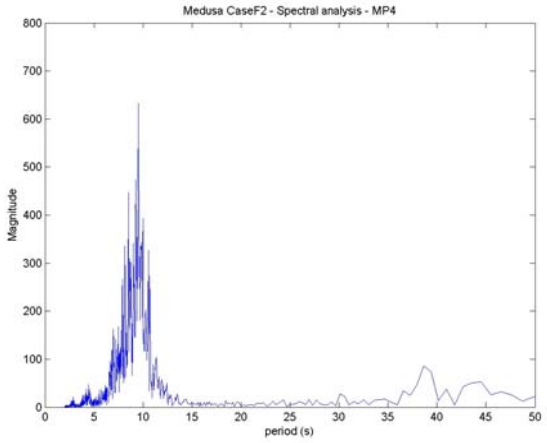

Monitoring point 4 – Spectrum

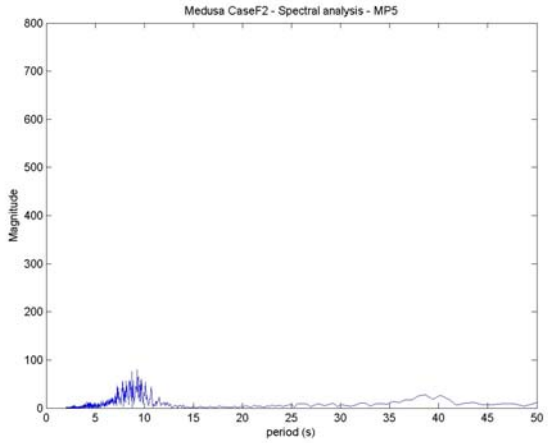

Monitoring point 5 – Spectrum

Figure 43: Pressure spectra – Medusa Spar – CaseF2

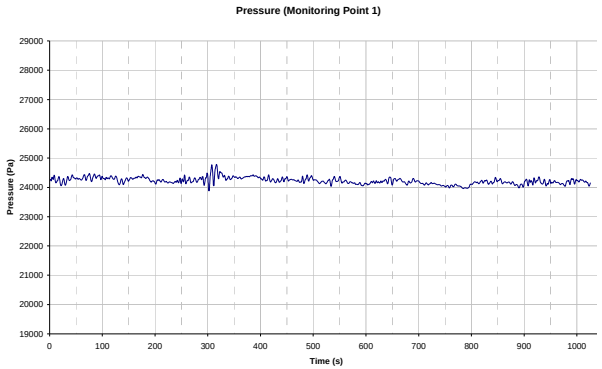

Monitoring point 1 – Pressure time histories

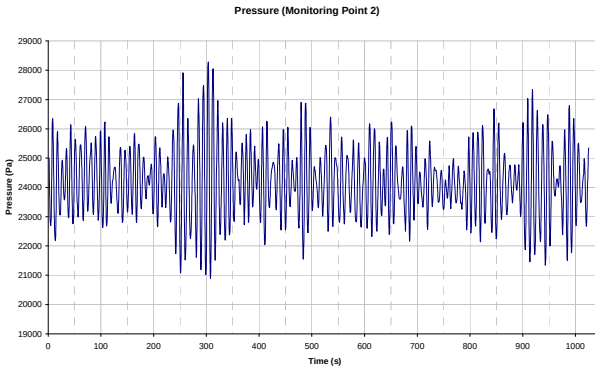

Monitoring point 2 – Pressure time histories

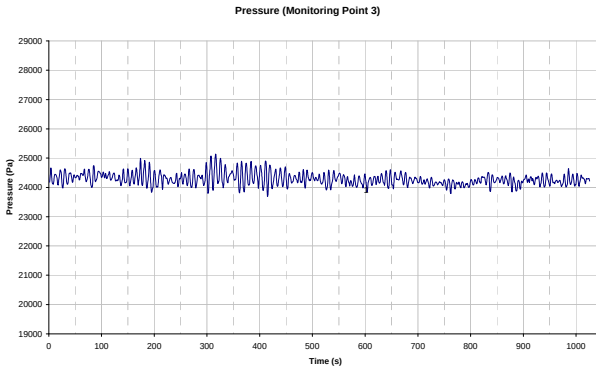

Monitoring point 3 – Pressure time histories

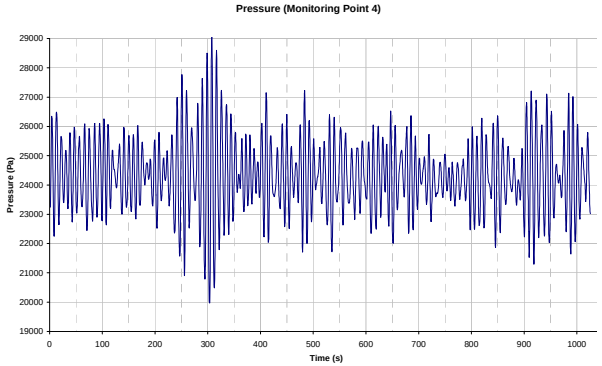

Monitoring point 4 – Pressure time histories

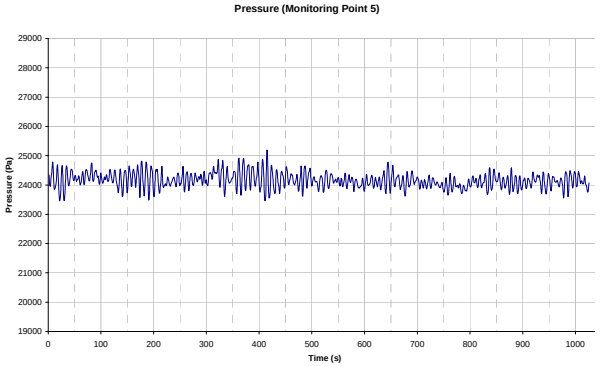

Monitoring point 5 – Pressure time histories

Figure 44: Pressure time histories – Medusa Spar – CaseF3

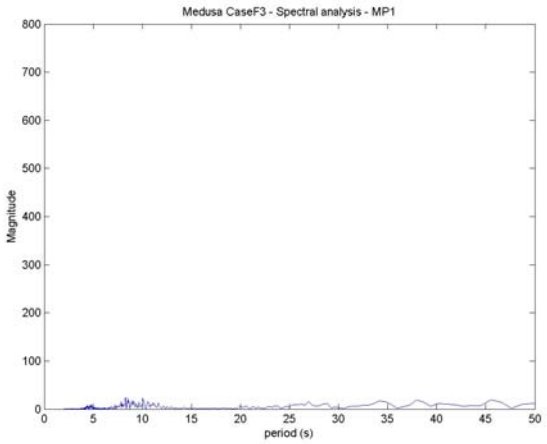

Monitoring point 1 – Spectrum

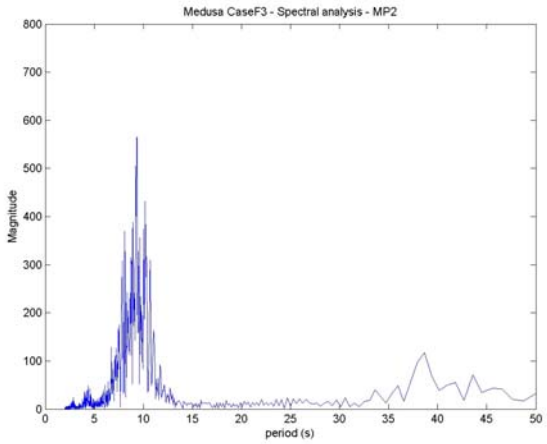

Monitoring point 2 – Spectrum

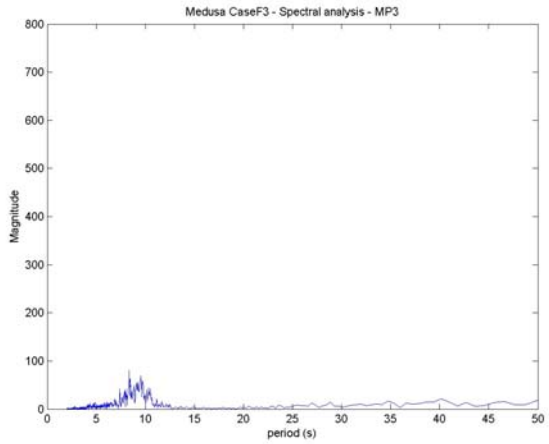

Monitoring point 3 – Spectrum

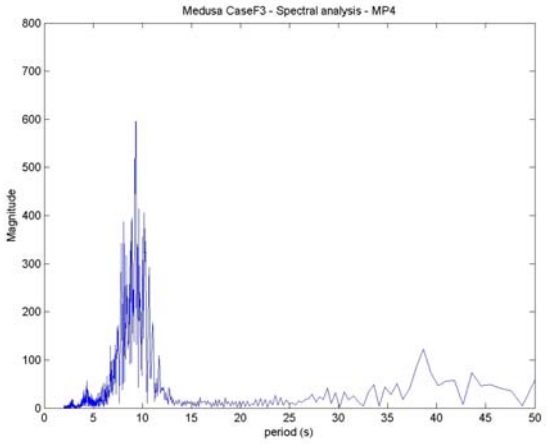

Monitoring point 4 – Spectrum

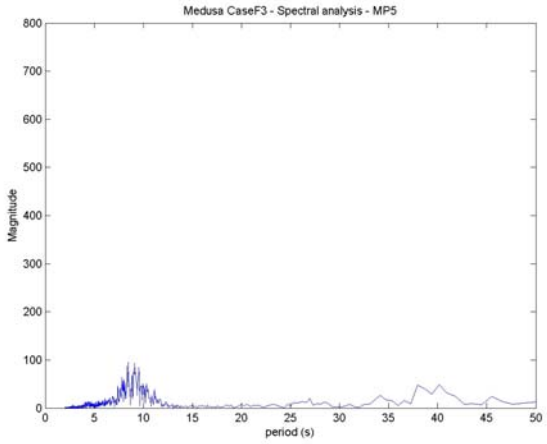

Monitoring point 5 – Spectrum

Figure 45: Pressure spectra – Medusa Spar – CaseF3

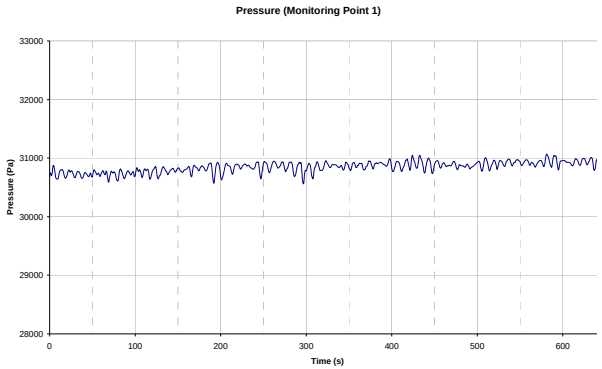

Monitoring point 1 – Pressure time histories

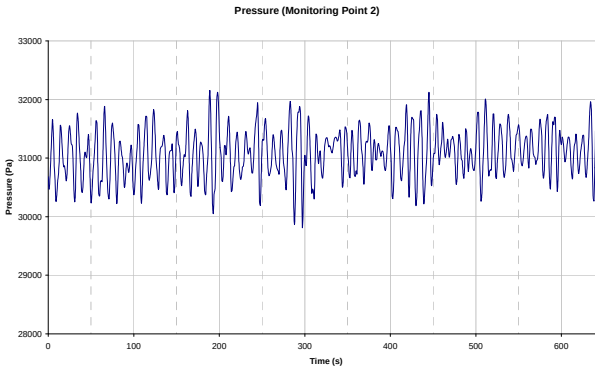

Monitoring point 2 – Pressure time histories

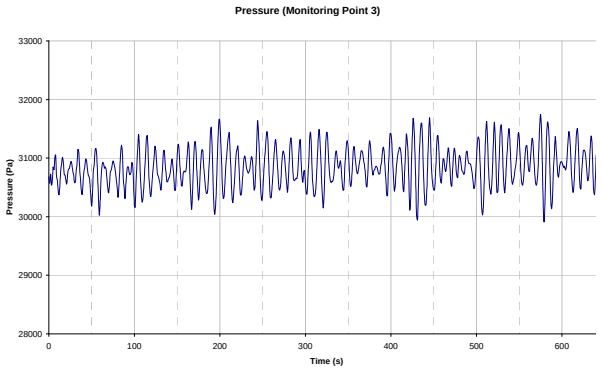

Monitoring point 3 – Pressure time histories

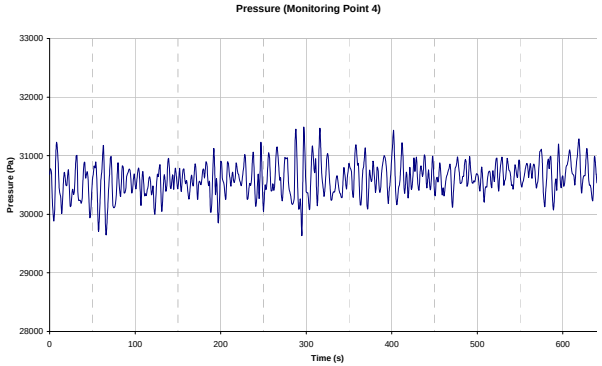

Monitoring point 4 – Pressure time histories

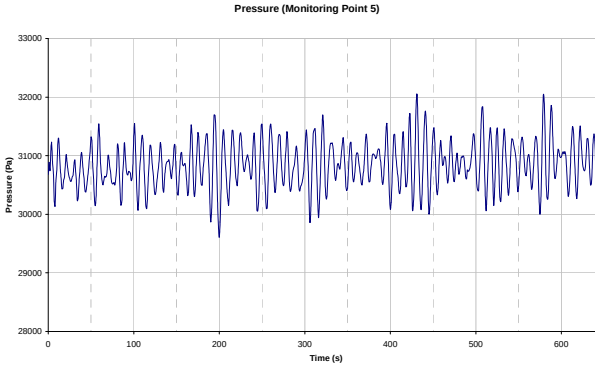

Monitoring point 5 – Pressure time histories

Figure 46: Pressure time histories – Front Runner Spar – CaseF10

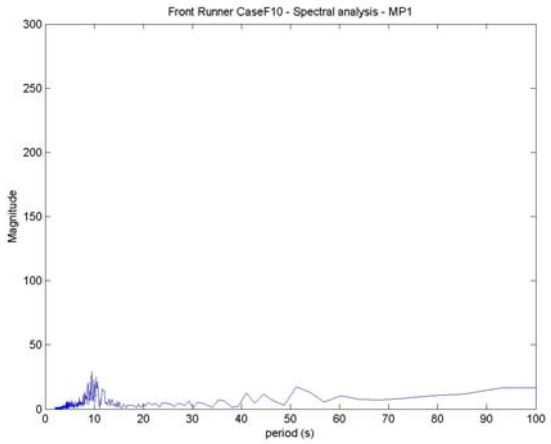

Monitoring point 1 – Spectrum

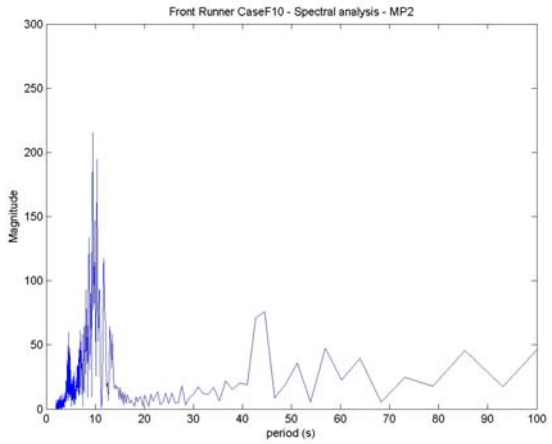

Monitoring point 2 – Spectrum

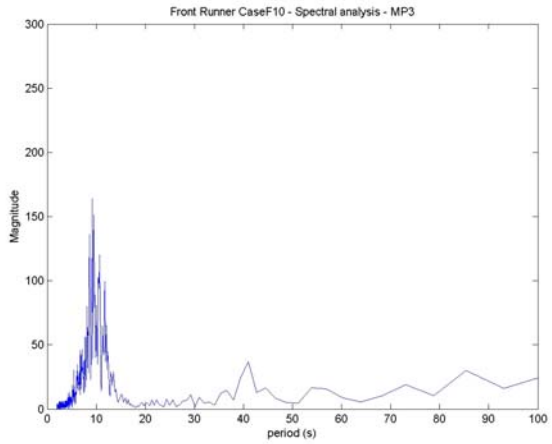

Monitoring point 3 – Spectrum

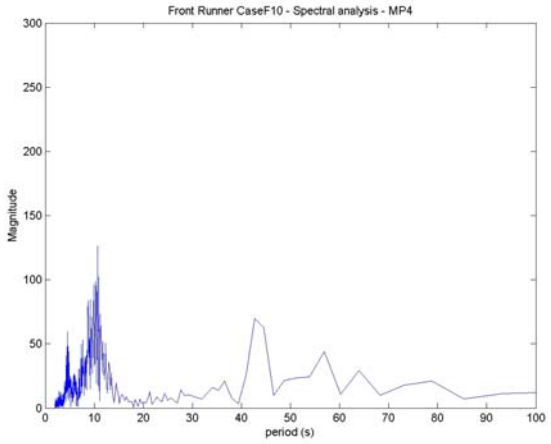

Monitoring point 4 – Spectrum

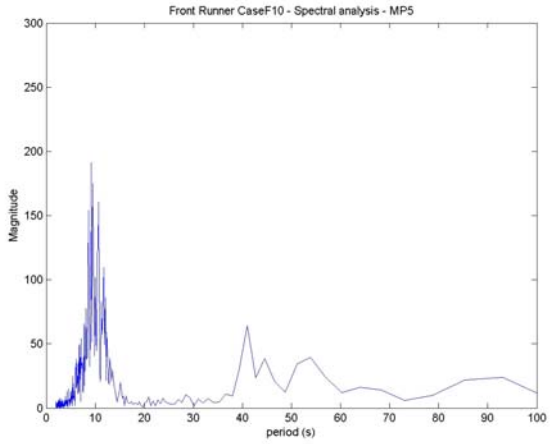

Monitoring point 5 – Spectrum

Figure 47: Pressure spectra – Front Runner Spar – CaseF10

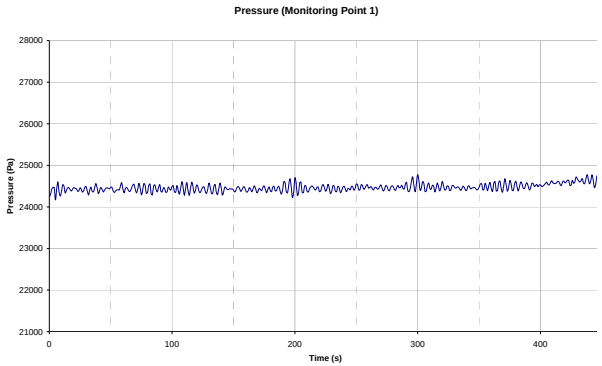

Monitoring point 1 – Pressure time histories

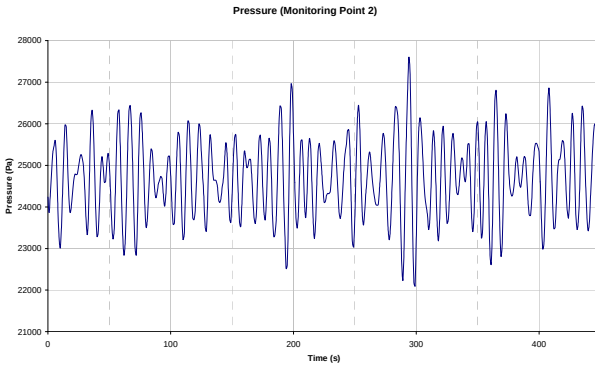

Monitoring point 2 – Pressure time histories

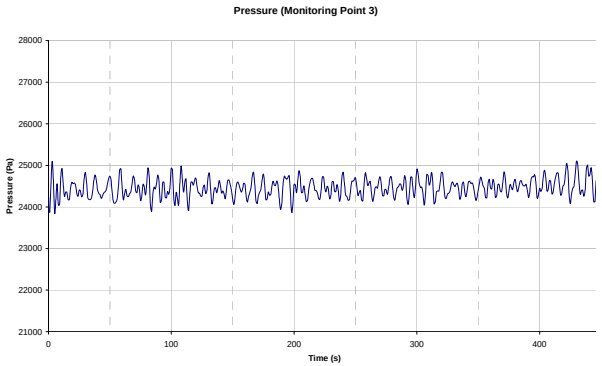

Monitoring point 3 – Pressure time histories

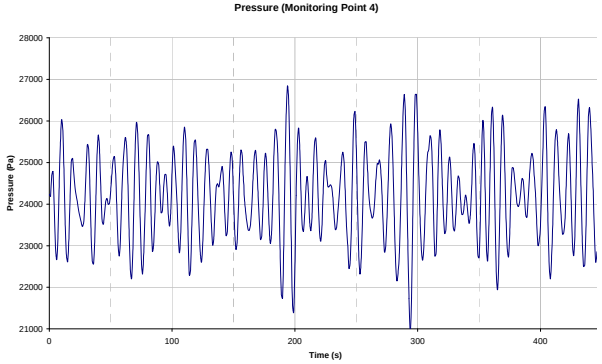

Monitoring point 4 – Pressure time histories

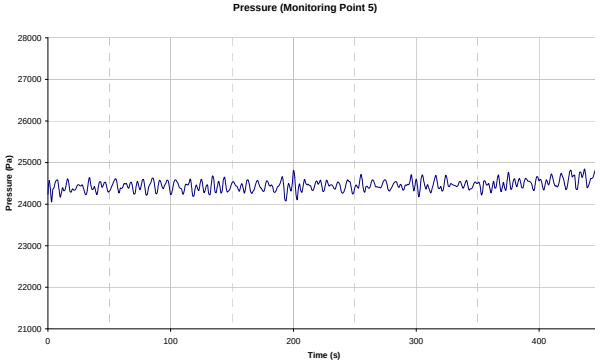

Monitoring point 5 – Pressure time histories

Figure 48: Pressure time histories – Front Runner Spar – CaseF16

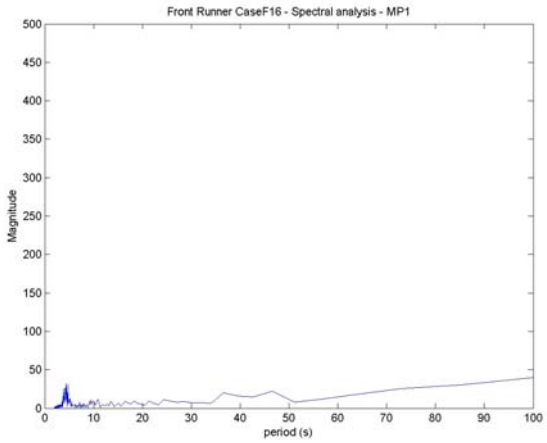

Monitoring point 1 – Spectrum

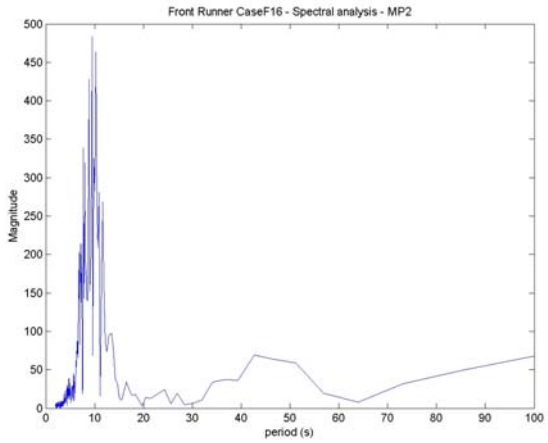

Monitoring point 2 – Spectrum

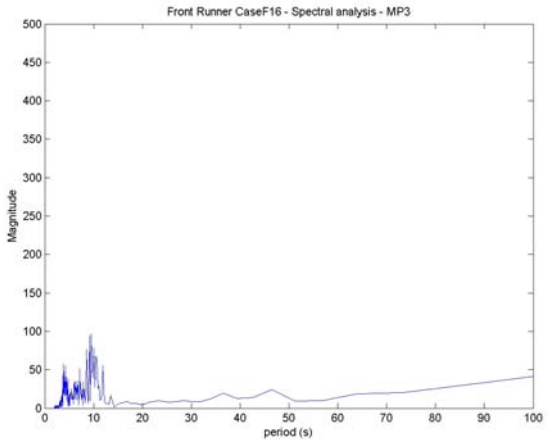

Monitoring point 3 – Spectrum

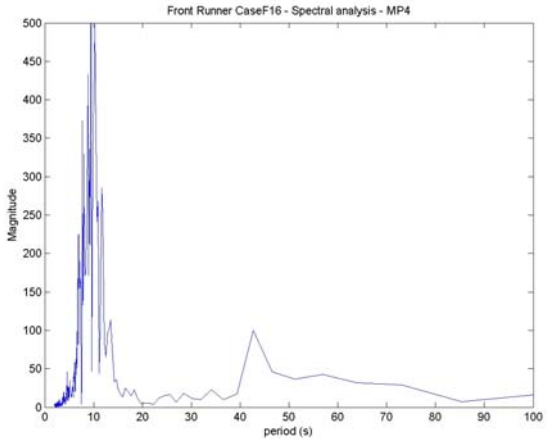

Monitoring point 4 – Spectrum

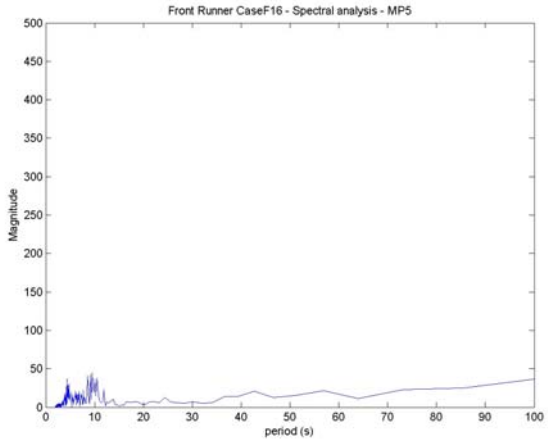

Monitoring point 5 – Spectrum

Figure 49: Pressure spectra – Front Runner Spar – CaseF16

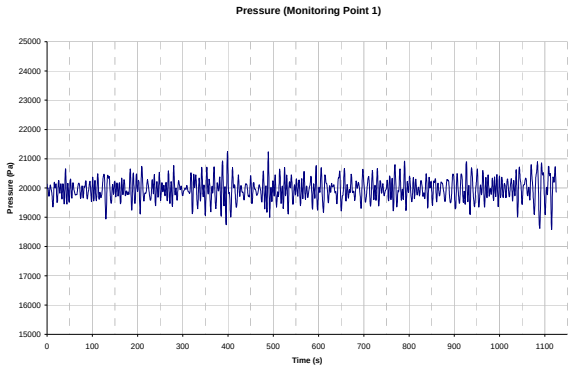

Monitoring point 1 – Pressure time histories

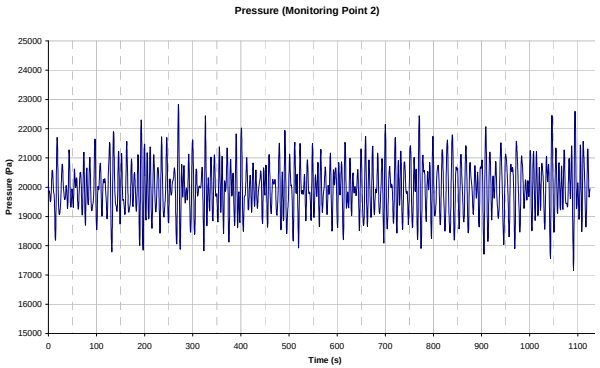

Monitoring point 2 – Pressure time histories

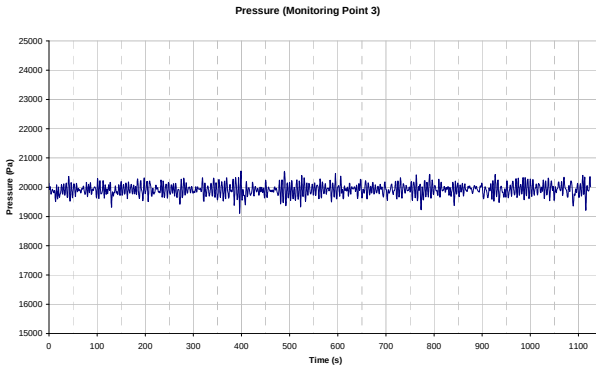

Monitoring point 3 – Pressure time histories

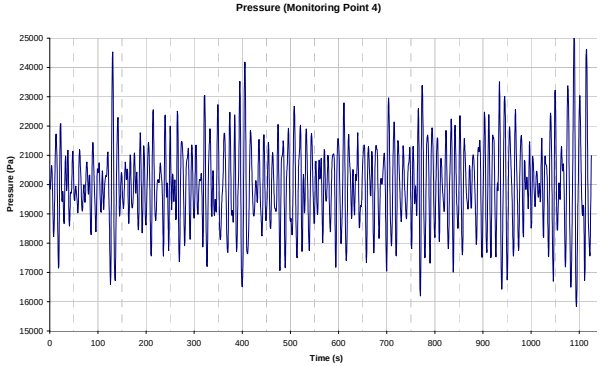

Monitoring point 4 – Pressure time histories

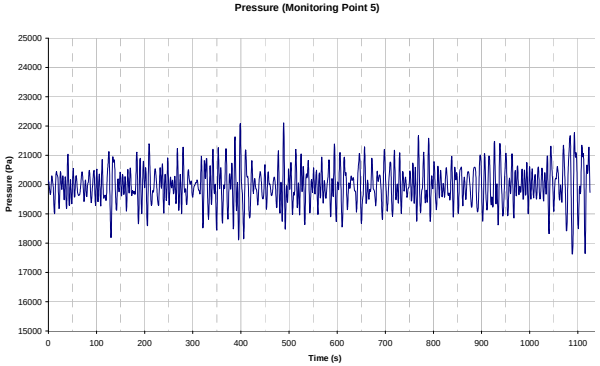

Monitoring point 5 – Pressure time histories

Figure 50: Pressure time histories – Marlin TLP – CaseF10

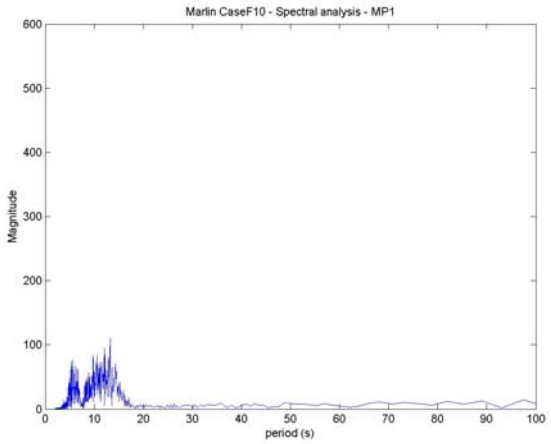

Monitoring point 1 – Spectrum

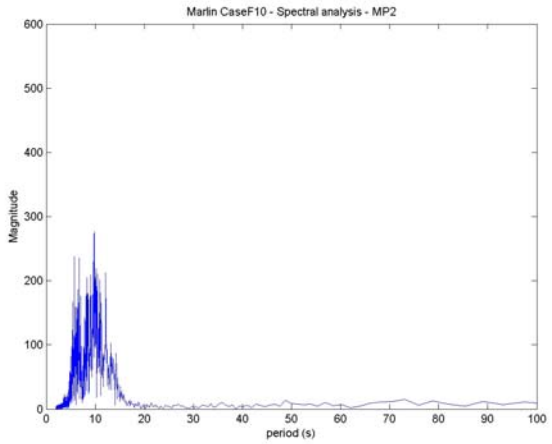

Monitoring point 2 – Spectrum

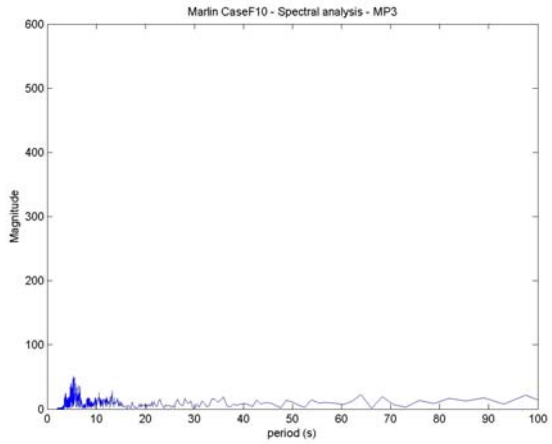

Monitoring point 3 – Spectrum

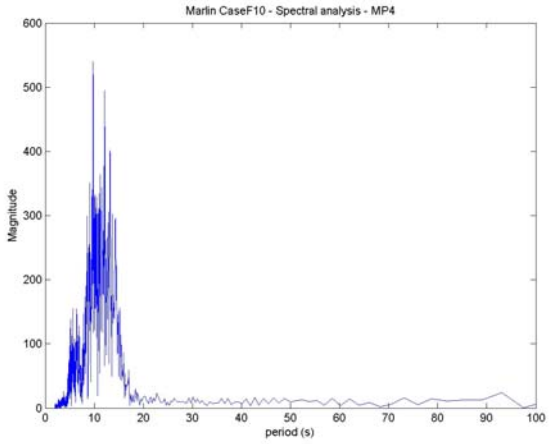

Monitoring point 4 – Spectrum

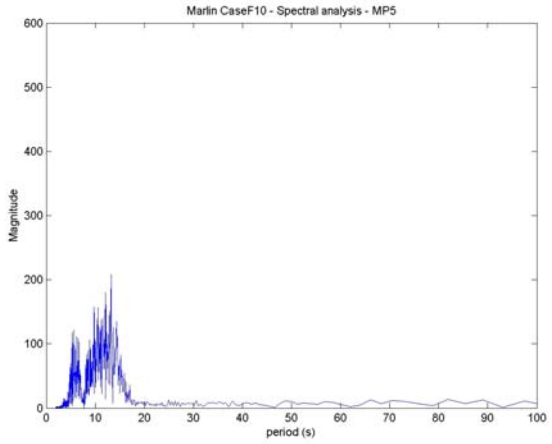

Monitoring point 5 – Spectrum

Figure 51: Pressure spectra – Marlin TLP – CaseF10

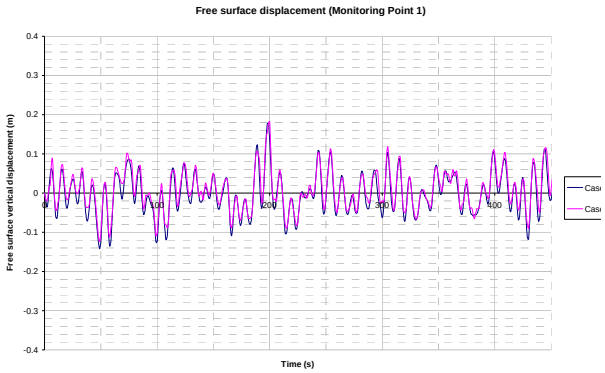

Monitoring point 1 – Free surface displacement

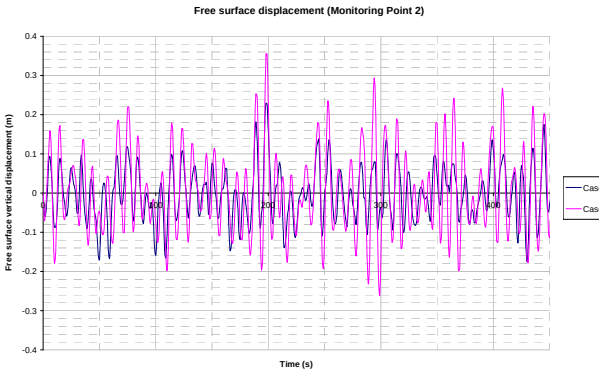

Monitoring point 2 – Free surface displacement

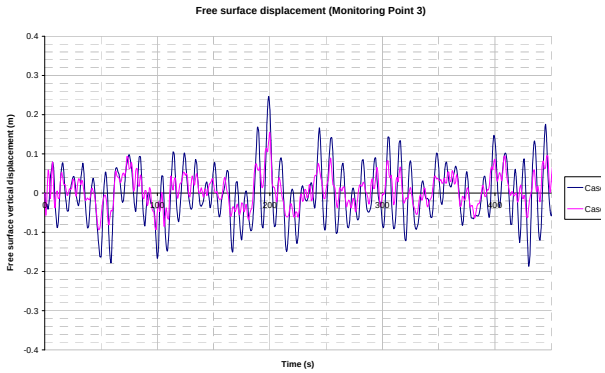

Monitoring point 3 – Free surface displacement

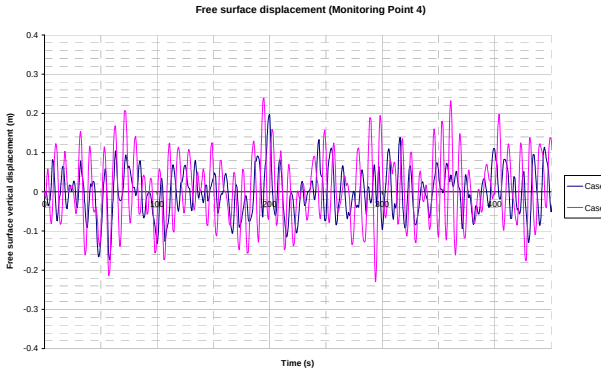

Monitoring point 4 – Free surface displacement

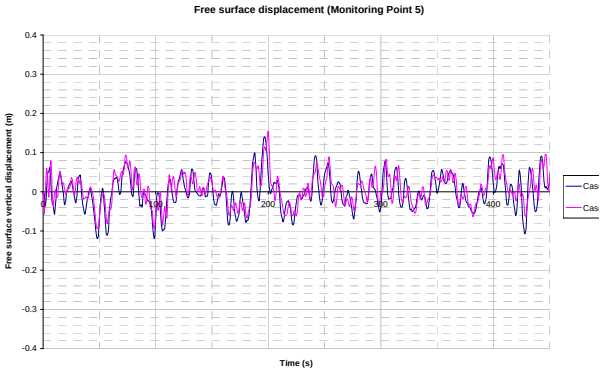

Monitoring point 5 – Free surface displacement

Figure 52: Free surface displacements – Front Runner Spar – Comparion CaseF10/CaseF16

9.6. Flow Visualizations

Some examples of sloshing and splashing for Medusa Spar are shown in Figure 53, and the velocity field for Marlin TLP, and Front Runner Spar are presented in Figure 54 and Figure 55, respectively.

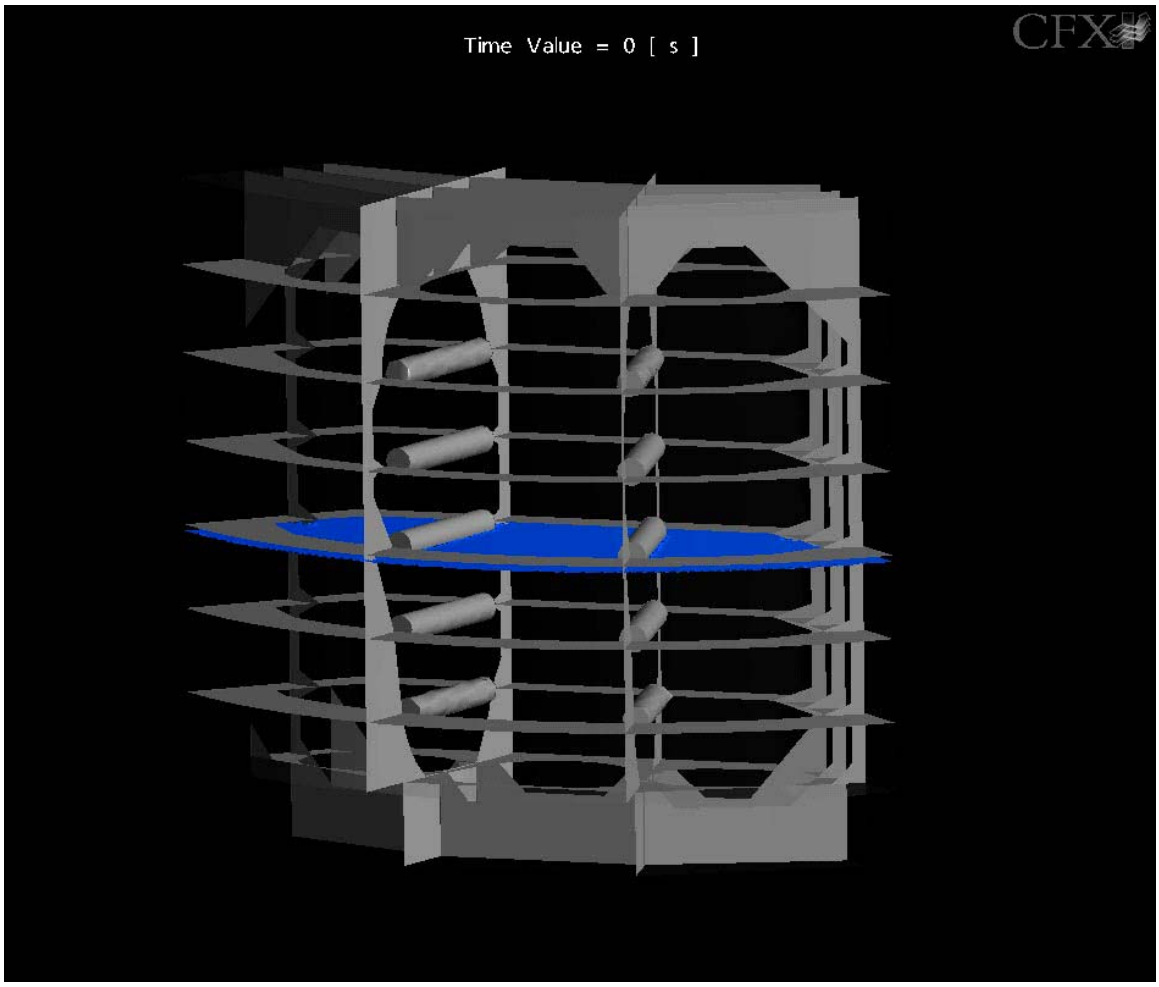

Figure 53:Sloshing and splashing in a ballast tank on Medusa Spar (see also the animated video "Animation Medusa CaseF2.mpg" provided on the CD.

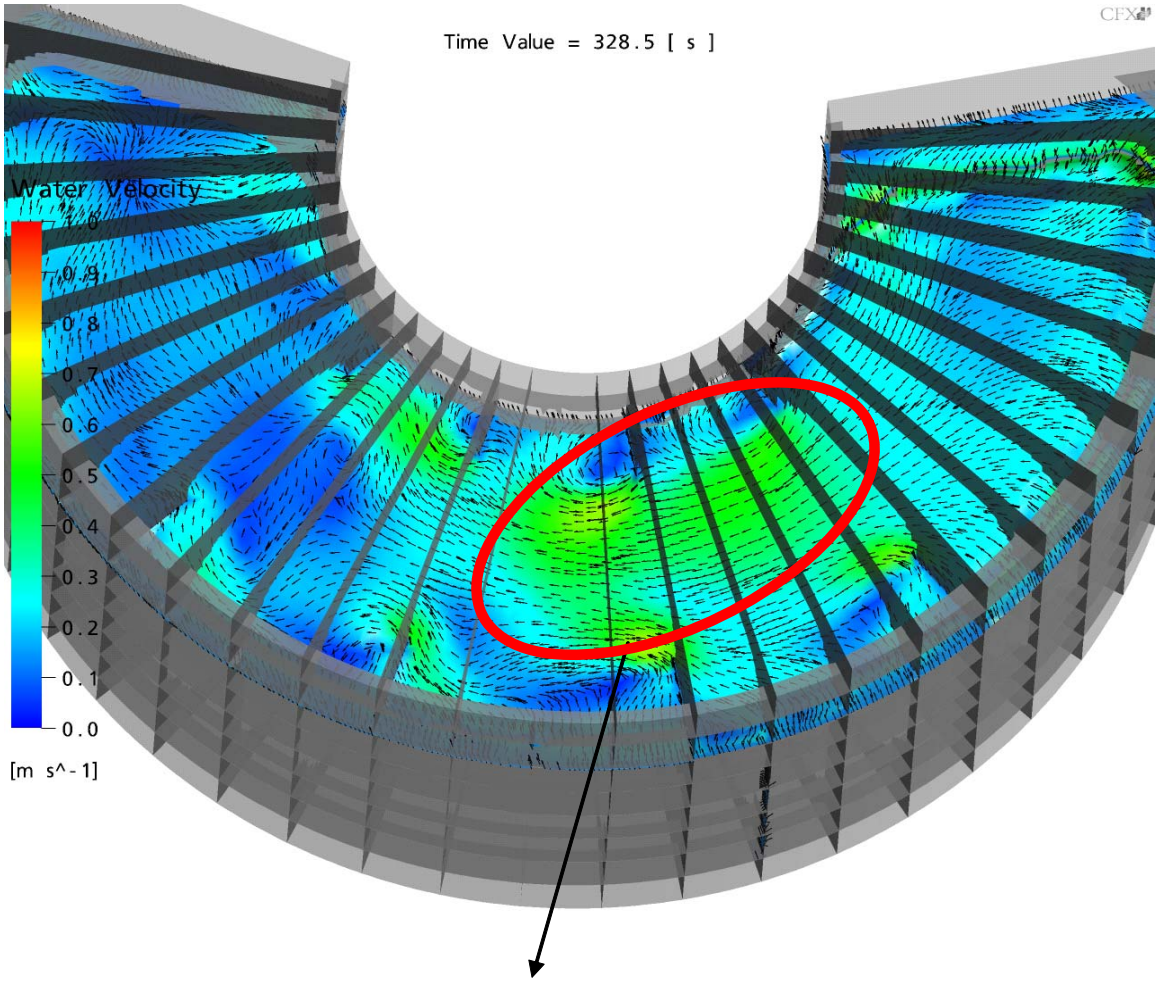

Figure 54: Water velocity field on free surface – Marlin TLP – CaseF10 (see also the animated video "Animation Marlin 3.mpg", provided on the CD)

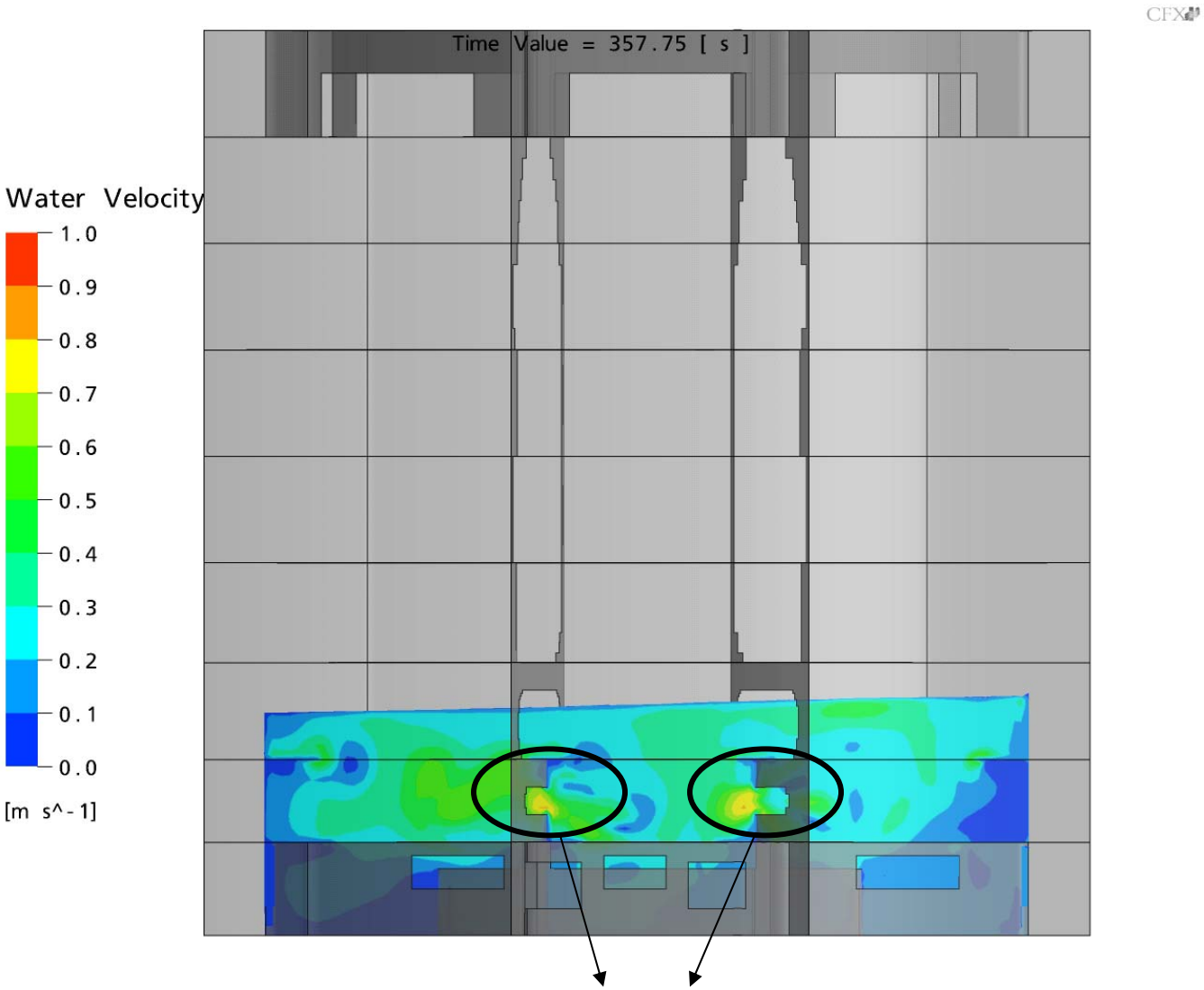

Figure 55: Water velocity field on vertical plane – Front Runner Spar – CaseF16 (see also the animated video "Animation Front Runner.mpg", provided on the CD)

10. Discussion and Conclusions

Task A

- The full-scale global motions of oil platforms at the location of a liquid tank have been derived from available real measurements on three deep ocean oil platforms: Medusa and Front Runner Spars and Marlin TLP. Six-degrees of freedom data are used for the spar tank and two degrees of freedom motion data are used for Marlin TLP. The pre-selected motion data from all platforms represent typical platform responses under moderate sea state conditions. The motion data are selected by examining at least of two years of continuous data. The final selection of data for the analyzed cases is limited to the events when the tank content (the mean level) did not change due to filling or emptying.

Task B

- In addition to the platform global motions that represent the main driving force for liquid commotion in the ballast tanks, the characteristic parameters of liquid motion -- elevation and frequencies -- are identified.
- The occurrence of sloshing in a tank has been identified in full-scale liquid level data using the methods such as wavelets and coherence spectra.

Task C

- The equivalent numerical CFD models have been built that match very fine details of the ballast tank prototypes. Not only was the overall geometry modeled, but also the structural members inside the tanks were modeled to capture complicated interferences between the liquid and the tank.
- The CFD model was validated using Medusa Spar data. Blind calculation of the liquid level in one of the Medusa Spar ballast tanks was performed. The analytical and measured results of the liquid levels in time domain match very well.
- The full-scale measured liquid level data are available only at one location in a tank. CFD calculations have been expanded for multi-point sensor system arrangement at five locations around the circumference and at the middle of the tank. Analytical results show that the location where the liquid level is calculated (measured) has a significant influence on the capability to detect liquid sloshing.
- Sensitivity tests using the CFD model for different levels of tank filling do not show significant differences in detecting liquid levels in ballast tanks for the normal fill levels. However, if the fill level coincides with the level where a horizontal ring-frame may be located, the ring-frame acts as a horizontal baffle and suppress the liquid excitations.

Task D

- Comparisons of full-scale and simulated data show a high degree of confidence for the numerical CFD modeling
- Compare simulated data for different liquid levels in a tank and identify trend in the results.
- Results show that sampling interval can affect the accuracy of dynamic liquid level measurements if the sampling intervals are longer than the excitation disturbances. In the case of an offshore platform, whether a spar or a TLP, the platform motions correlate well with waves (even though the platform motions are negligibly small) within the expected wave period range of 4 to 15 seconds (see Figure 56). Thus, a 20-second sampling interval that is of the main

concern for MMS, is too long for the dynamic measurements of the liquid level in a tank. It is not recommended to set the liquid level sensors to operate at intervals that are longer than half the expected wave period (2 seconds). The sampling intervals that are in place on the platforms used in this study are appropriate. For some other platforms and different types of tanks, the longest allowable sampling intervals should be determined based on either the measurements or a careful CFD modeling. The appropriate solution for recommending the sampling rates that would not trigger false alarms should be defined on a case by case basis, taking into account the nature of the problem and the geometry of the tank.

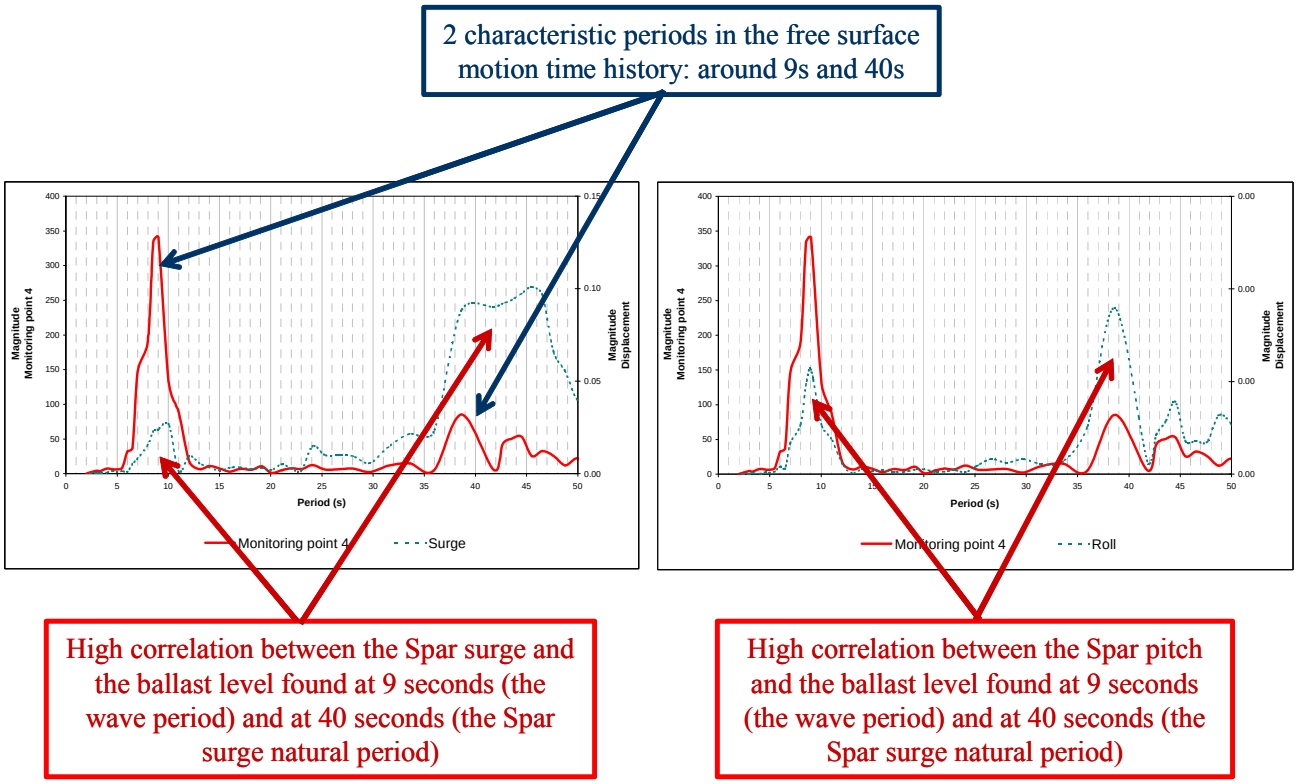

Figure 56: Two primary liquid level responses in the ballast tanks

The effect of sampling interval on detecting liquid sloshing can be visualized based on the following simplified example, shown in Figure 57 and Figure 58. For example, in a rectangular tank of the length of 60 feet, a progressive wave of small amplitude is generated by combining a standing wave and a Gaussian progressive disturbance packet. This model is similar to an impulsive wave model with a "crest" traveling from one side of the tank to another. A level probe at the left end of the tank is set to measure the surface elevation at a prescribed sampling interval. Based on the sampling intervals of 1 and 20 seconds (see Figure 58), the measured time series of the surface elevation at a fix location are different, as expected.
On the other hand, if the primary goal is to monitor the amount of liquid in the tank for leaking, it is recommended to use longer sampling intervals. This would result in smoother and more stable running average values (see the measured points and the running average curve in Figure 58), so the free surface sloshing would not affect the level regulators. If the sampling time was reduced, the results would be just the opposite. However, the criteria for sampling rate need to be determined based on actual tank properties and the purpose of liquid level measurement.

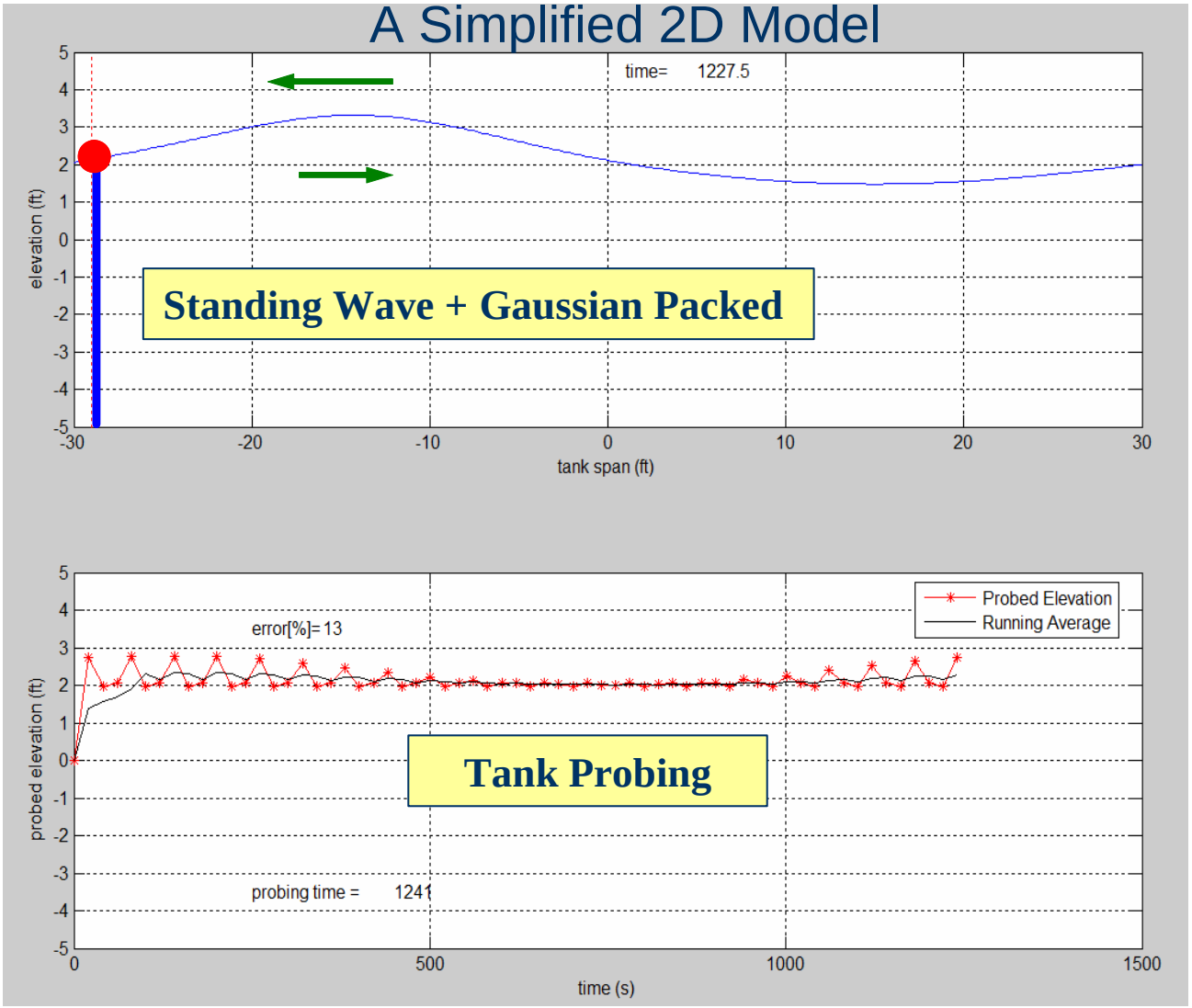

Figure 57: A snapshot of thef free surface profile during sloshing and the measuring probe (red ball) (upper); Measure free surface elevation at the probe location and the running average of the measured points (lower)

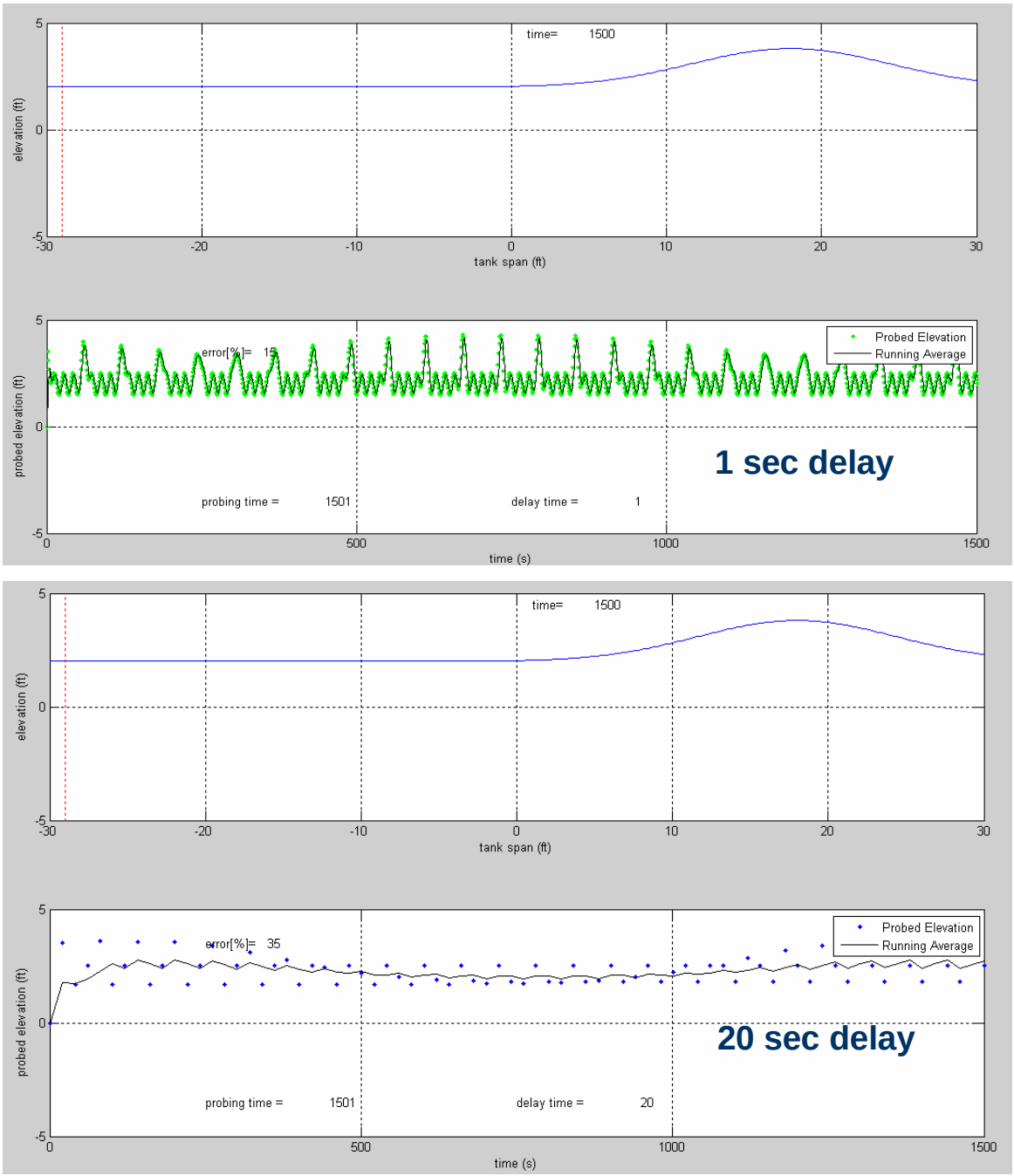

Figure 58: A snapshot of thef free surface profile during sloshingand the measure free surface elevation at the probe location sampled a 1s (upper) and 20 s intervals (lower) with the associated running averages

- The sensor location along the tank boundary is also relevant for the accuracy of liquid level measurements. If the sensors were placed at the "nodes" rather than at the "antinodes", the sloshing would not be detected. In addition, as the sloshing parameters depend on the amount of liquid in the tank, the location of the "nodes" would also vary with the amount of liquid. Thus, it is not advisable to rely on putting the sensors at nodal points, unless the amount of liquid does not change. The nodal points can be easily determined analytically using a CFD model.

- In conclusion, the existing CFD CFX code can be successfully used to model and predict the behavior of a liquid in ballast tanks on spars and TLPs. However, the cases that we discussed here are specific to the ballast tanks on the most common offshore platforms: spars and TLPs. If different types of platforms or ships, e.g., the LNG carriers, with tanks of different shapes and internal compartmentalization are of interest, the liquid sloshing dynamics can be of different nature. Consequently, the conclusions derived from this study can be different. Nevertheless, the CFD is a powerful method, computationally time demanding, but if modeled correctly, the sloshing effects can be predicted reliably and the time delays can be incorporated into the alarm system to prevent spurious alarms.

- If the provided solutions are not fully applicable, a remedy for "false" alarms can be found in real-time measurements supported by an expert system, such as a neural network advisory system. If this system is properly trained, it can provide solutions in real time for a variety of conditions that are difficult to address using conventional analytical methods (including CFD) during the design process.

11. Acknowledgment

This study was funded by the Minerals Management Service, U.S. Department of the Interior, Washington, D.C., under Contract Number 1435-01-05-CT-39120. It was also made possible through generosity and support of BP America Production Company and Murphy Oil Corporation. Both companies provided data without which this study would not have been possible. Special gratitude goes to Mr. Thomas von Aschwege, Mr. Steve Perryman, and Dr. Pierre Liagre from BP America and to Mr. Paul Fourchy and Mr. Steve Green from Murphy Oil. Their help in locating data and data-based information was invaluable.

12. References

Edwards, R.; I. Prislin, T. Johnson, C. Campman, S. Leverette, J. Halkyard: "Review of 17 Real-Time, Environment, Response, and Integrity Monitoring Systems on Floating Production Platforms in the Deep Waters of the Gulf of Mexico", OTC Paper # 17650, Houston 2005

Faltinsen, O. M.; O.F. Rognebakke; A.N. Timokha: "Resonant three-dimensional nonlinear sloshing in a square-base basin", J. Fluid Mech. (2003), vol. 487, pp. 1–42.

Ibrahim, R.A.: "Liquid Sloshing Dynamics – Theory and Applications", Cambridge University Press, 2005

Lamb, H. "Hydrodynamics", 6th ed., Cambridge University Press, reprint 1997

Standing, R, S. Amaratunga, F.L.C. Calleja, R. Eichaker, and S. Orme: “Marine hydrodynamics modeling using CFD”, CFD Technology in Ship Hydrodynamics Conference, London, January 2003

Van Dyke, M.: “An Album of Fluid Motion”, Parabolic Press, Stanford, 1982